

Optic flow-based collision-free strategies: From insects to robots

Julien Serres, Franck Ruffier

▶ **To cite this version:**

Julien Serres, Franck Ruffier. Optic flow-based collision-free strategies: From insects to robots. Arthropod Structure and Development, 2017, 46 (5), pp.703 - 717. 10.1016/j.asd.2017.06.003 . hal-01644523

HAL Id: hal-01644523
https://amu.hal.science/hal-01644523

Submitted on 22 Nov 2017

HAL is a multi-disciplinary open access archive for the deposit and dissemination of scientific research documents, whether they are published or not. The documents may come from teaching and research institutions in France or abroad, or from public or private research centers.

L'archive ouverte pluridisciplinaire **HAL**, est destinée au dépôt et à la diffusion de documents scientifiques de niveau recherche, publiés ou non, émanant des établissements d'enseignement et de recherche français ou étrangers, des laboratoires publics ou privés.

Arthropod Structure & Development 46 (2017) 703–717

Contents lists available at ScienceDirect

Arthropod Structure & Development

journal homepage: www.elsevier.com/locate/asd

Review article

Optic flow-based collision-free strategies: From insects to robots

Julien R. Serres*, Franck Ruffier

Aix Marseille Univ, CNRS, ISM, Marseille, France

ARTICLE INFO

Article history:
Received 7 July 2016
Received in revised form
19 June 2017
Accepted 19 June 2017
Available online 11 July 2017

Keywords:
Optic flow
Insect flight
Obstacle avoidance
Speed control
Short-range navigation
Biorobotics
Biomimicry
Bionics

ABSTRACT

Flying insects are able to fly smartly in an unpredictable environment. It has been found that flying insects have smart neurons inside their tiny brains that are sensitive to visual motion also called optic flow. Consequently, flying insects rely mainly on visual motion during their flight maneuvers such as: takeoff or landing, terrain following, tunnel crossing, lateral and frontal obstacle avoidance, and adjusting flight speed in a cluttered environment. Optic flow can be defined as the vector field of the apparent motion of objects, surfaces, and edges in a visual scene generated by the relative motion between an observer (an eye or a camera) and the scene. Translational optic flow is particularly interesting for short-range navigation because it depends on the ratio between (i) the relative linear speed of the visual scene with respect to the observer and (ii) the distance of the observer from obstacles in the surrounding environment without any direct measurement of either speed or distance. In flying insects, roll stabilization reflex and yaw saccades attenuate any rotation at the eye level in roll and yaw respectively (i.e. to cancel any rotational optic flow) in order to ensure pure translational optic flow between two successive saccades. Our survey focuses on feedback-loops which use the translational optic flow that insects employ for collision-free navigation. Optic flow is likely, over the next decade to be one of the most important visual cues that can explain flying insects' behaviors for short-range navigation maneuvers in complex tunnels. Conversely, the biorobotic approach can therefore help to develop innovative flight control systems for flying robots with the aim of mimicking flying insects' abilities and better understanding their flight.

© 2017 The Authors. Published by Elsevier Ltd. This is an open access article under the CC BY license (http://creativecommons.org/licenses/by/4.0/).

1. The biorobotic approach: a transdisciplinary approach

While the biological substrate has not yet been fully identified (Webb and Wystrach, 2016), the biorobotic approach is particularly useful both in the fields of Neuroscience and Robotics (Beer et al., 1998; Franz and Mallot, 2000; Webb, 2001, 2006; Landgraf et al., 2010; Srinivasan, 2011; Floreano et al., 2014; Ijspeert, 2014; Franceschini, 2014), because the robotic model can be tested in similar experimental conditions like ethological experiments and suggest new biological hypotheses. From these iterations between robotic and ethological experiments, we can remove uncertainties about the navigation model by considering the minimum requirements to perform navigational tasks (e.g.: Franceschini et al., 1992; Lambrinos et al. (2000); Horchler et al. (2004); Franceschini et al. (2007); Roubieu et al. (2014); Hartbauer (2017)). The biorobotic approach enables us “to kill two birds with one stone”, because it yields elegant robotic solutions which require far fewer sensors, computational resources, and storage capabilities than conventional robotic approaches, while providing a possible explanation for free-flying insects’ abilities to travel safely through an unknown environment, thereby suggesting functions in the biological substrate.

This review provides an overview of optic flow-based collision-free strategies with a biorobotic viewpoint. Flying insects rely heavily on optic flow to detect and avoid obstacles in an unpredictable environment, consequently a focus will be drawn on optic flow-based strategies. Over the last 25 years, a huge amount of research into optic flow-based robotics has been carried out to achieve a better understanding of how insects may exploit optic flow during their flight. We will exhaustively describe this research in this review. In Section 2, optic flow will be introduced as a visual cue which depends on both the environment's configuration and the animal's own movement. In Section 3, the biological substrate of optic flow sensing in flying insects will be introduced. In Section 4, the chicken-and-egg problem of translational optic flow will be posed. In Sections 5 and 6, optic flow-based strategies either in the horizontal plane or in the vertical plane will be respectively detailed. In Section 7, the other visual cues explaining insect flight

* Corresponding author.
E-mail address: julien.serres@univ-amu.fr (J.R. Serres).

http://dx.doi.org/10.1016/j.asd.2017.06.003
1467-8039/© 2017 The Authors. Published by Elsevier Ltd. This is an open access article under the CC BY license (http://creativecommons.org/licenses/by/4.0/).

will be introduced. In Section 8, a conclusion will be drawn suggesting the possibility of bioroboticists using insect-sized robots to test biological hypotheses at the scale of a flying insect.

2. What is optic flow?

The optic flow vector field perceived by an agent (an animal, a robot, or a human) is particularly dependent on the structure of the environment (Gibson, 1950; Whiteside and Samuel, 1970; Nakayama and Loomis, 1974; Koenderink and van Doorn, 1987; Krapp Hengstenberget al, 1996). Optic flow can be defined by a vector field of the apparent motion of objects, surfaces, and edges in a visual scene caused by the relative motion between an agent and the scene (Fig. 1). The optic flow field $\overrightarrow{\omega}$ (1) is the combination of two optic flow components: a translational optic flow $\overrightarrow{\omega_T}$ and a rotational optic flow $\overrightarrow{\omega_R}$ (Koenderink and van Doorn, 1987).

$$\overrightarrow{\omega} = \overrightarrow{\omega_T} + \overrightarrow{\omega_R} \quad (1)$$

Rotational optic flow depends only on the agent's own rotations. However in the horizontal plane, translational optic flow, which describes the front-to-back motion occurring when the agent moves forward, depends on the ratio between the relative linear speed V and the distance D_φ from the contrasting objects of the environment, and the angle φ between the gaze direction and the speed vector (2).

$$\omega_T = \frac{V}{D_\varphi} \cdot sin(\varphi) \quad (2)$$

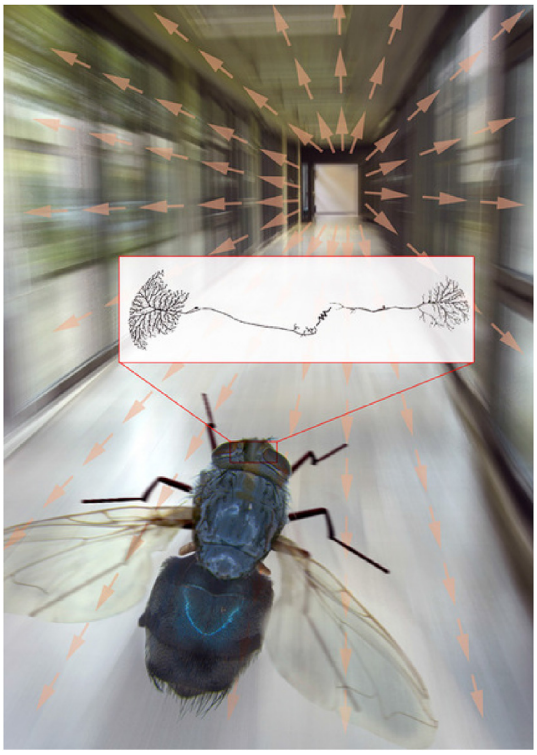


Fig. 1. Optic flow field for a fly flying straight ahead along a corridor produces, through its movement, a vector field of the apparent motion of corridor surfaces. This optic flow field is then processed on a higher level of the visual ganglia, called the Lobula Plate Tangential Cells -LPTC- neurons, so as to correct the flight course. Turns are controlled by the direct connection of two nerves, the HSE LPTC-neuron (right) and the H2 LPTC-neuron (left). ©Robert Schorner – PhotoLab/Max Planck Institute of Neurobiology (Farrow et al., 2006).

Translational optic flow (2) is particularly interesting for short-range navigation because it depends on the ratio between (i) the relative linear speed of an object in the scene with respect to the agent and (ii) the distance from obstacles in the surrounding environment: this visual angular speed cue does not require either speed or distance measurement (2).

3. How are flying insects sensitive to optic flow?

In flies, the third optic ganglion, called the Lobula Plate, appears as a genuine "visual motion processing center". It comprises approximately 60 uniquely identifiable neurons, the Lobula Plate Tangential Cells - LPTCs-neuron – that respond to the optic flow pattern resulting from the animal motion, and transmit the signal via the neck to thoracic interneurons (Hausen, 1982; Strausfeld and Bassemir, 1985; Krapp and Hengstenberg, 1996; Krapp et al., 1998; Borst and Haag, 2002; Egelhaaf and Kern, 2002; Strausfeld, 2012) (see also review Taylor and Krapp (2007)). The LPTCs are large-field collator neurons that pool the input signals from many retinotopic "Elementary Motion Detectors" (EMDs) (Hausen, 1982; Borst and Haag, 2002; Egelhaaf and Kern, 2002). By integrating these input signals, and through lateral interactions within the bilateral Lobula Plate system (Hausen, 1982; Farrow et al., 2006) (Fig. 1), LPTCs have complex receptive fields fitting with optic flow-field patterns induced by different flight maneuvers (Krapp and Hengstenberg, 1996; Krapp et al., 1998). LPTCs-neuron are involved either in the detection of rotational optic flow patterns (e.g., HS- and VS-neurons Krapp and Hengstenberg (1996); Krapp et al. (1998); Taylor and Krapp (2007)) or translational optic flow patterns (e.g., H1-neuron Franceschini et al. (1989), Hx-neuron Krapp and Hengstenberg (1996); Krapp et al. (1998), or HSE- and H2-neuron in Farrow et al. (2006)). In flies, LPTCs also respond to local visual motion: an apparent motion in front of only two photoreceptors is necessary and sufficient to elicit a consistent activity of the H1-neuron (Franceschini et al., 1989). This local sensitivity seems to be based on the early separation of ON contrast and OFF contrast detection (ON: from dark to bright; OFF: from bright to dark) (Franceschini et al., 1989; Eichner et al., 2011) and seems to be a general principle in motion vision for vertebrates and invertebrates (Borst and Helmstaedter, 2015). In honeybees, the so-called Velocity-Tuned neurons (VT-neuron) are known to respond monotonically with the visual angular speed (Ibbotson, 2001).

In locusts, the Lobula Giant Movement Detector – LGMD-neuron – is a bilaterally paired motion sensitive neuron that collects local motion measurements coming from the second optic ganglion, called the Medulla, which forms a synapse with the Descending Contralateral Movement Detector – DCMD-neuron – (Rind, 1984; Rind and Simmons, 1992; Rind and Bramwell, 1996). The DCMD neurons respond robustly to looming objects and are responsible for triggering predator escape and collision avoidance behaviours in locusts (Rind, 1987; Rind and Simmons, 1997; Gabbiani et al., 1999; Rind et al., 2008; Gray et al., 2010).

4. The chicken-and-egg problem of the translational optic flow

A given value of translational optic flow is a kind of chicken-and-egg problem (2), because an infinite number of couples (speed; distance) lead to the same speed/distance ratio, i.e. the same optic flow value. For instance, an optic flow value of 1 rad/s (i.e., 57°/s) can be generated by an agent moving at 1 m/s at 1 m from an obstacle, or moving at 2 m/s at 2 m from an obstacle, and so on (see Fig. 2). To get around the optic flow chicken-and-egg problem, roboticists introduced the assumption prevailing in those days that robots have to measure their own speed by using a tachymeter on

wheels (Franceschini et al., 1992), a GPS unit (Griffiths et al., 2007), or a custom-built pitot tube (Beyeler et al., 2009), in order to assess the distance from obstacles, then to avoid them. However, flying insects are not able to directly measure their true groundspeed or their distance from obstacles. As far as we know for short-range navigation, insects do not solve the optic flow chicken-and-egg problem but instead use strategies directly based on optic flow patterns or criteria for collision-free navigation.

5. Optic flow-based guidance in the horizontal plane

5.1. Controlling flight speed by regulating the bilateral optic flow

The idea of introducing a speed control system based on optic flow was firstly developed by Coombs and Roberts (1992) in the field of Robotics. The mobile robot, called *Bee-Bot*, adjusted its forward speed by keeping the optic flow within a measurable range, using a bilateral optic flow criterion to control the robot's speed (Coombs and Roberts, 1992). The bilateral optic flow criterion (sum of the left and right optic flows) as a feedback signal to directly control speed was first introduced by Santos-Victor and colleagues (Santos-Victor et al., 1995) on-board the bee-inspired mobile robot, *Robee*. *Robee* was fitted with a pair of cameras to measure the right and left optic flows in a tapered corridor (Santos-Victor et al., 1995), and its speed control system was tuned by an optic flow-based algorithm. Qualitatively, *Robee*'s speed was scaled by the level of the environment's visual clutter. Bilateral optic flow criterion as a feedback signal to directly control the speed has since been tested on many robots in both straight and tapered corridors (Santos-Victor et al., 1995; Weber et al., 1997; Srinivasan et al., 1999; Baratoff et al., 2000; Argyros et al., 2004; Humbert et al., 2007; Humbert and Hyslop, 2010; Roubieu et al., 2012, 2014). The desired bilateral optic flow was ~12°/s for the *Bee-Bot* robot (Santos-Victor et al., 1995), ~19°/s in (Weber et al., 1997), ~46°/s in (Baratoff et al., 2000), ~21°/s in (Argyros et al., 2004), 190°/s or 250°/s in (Roubieu et al., 2012, 2014). The higher the desired bilateral optic flow, the more rapidly the robot went forward while moving close to the walls.

Conversely, robotic experiments can also suggest similar biological experiments. Bees appear to use a similar optic flow-based strategy to control their flight speed in a tapered corridor (Srinivasan et al., 1996), or in straight corridors in which the texture had been manipulated (Baird et al., 2005, 2006), or in a complex tunnel (Portelli et al., 2011) (Fig. 3a–d). When a bee flies through a tapered tunnel, it decreases its flight speed when the tunnel narrows, and increases it when the tunnel widens, in such a way that the bilateral optic flow (sum of the optic flow coming from the walls) remains constant at about 430°/s – 640°/s (Srinivasan et al., 1996; Baird et al., 2005). This observation suggests that bees may be equipped with a kind of optic flow regulator to adjust their flight speed by monitoring and regulating the optic flow perceived by their motion sensitive system (Serres et al., 2006, 2008b; Roubieu et al., 2014) (Fig. 7). Consequently, if the corridor width is

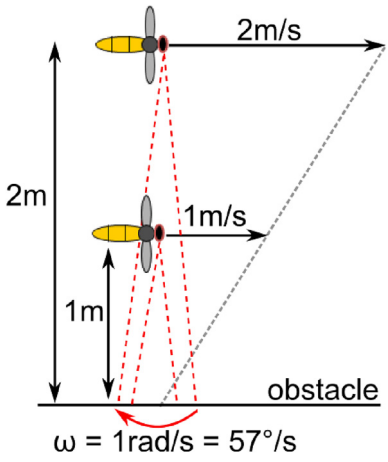


Fig. 2. The chicken-and-egg problem of the translational optic flow. An infinite number of couples (speed; distance) lead to the same speed/distance ratio, so the same angular velocity (optic flow magnitude). For instance in this picture an optic flow value of 1 rad/s (or 57°/s).

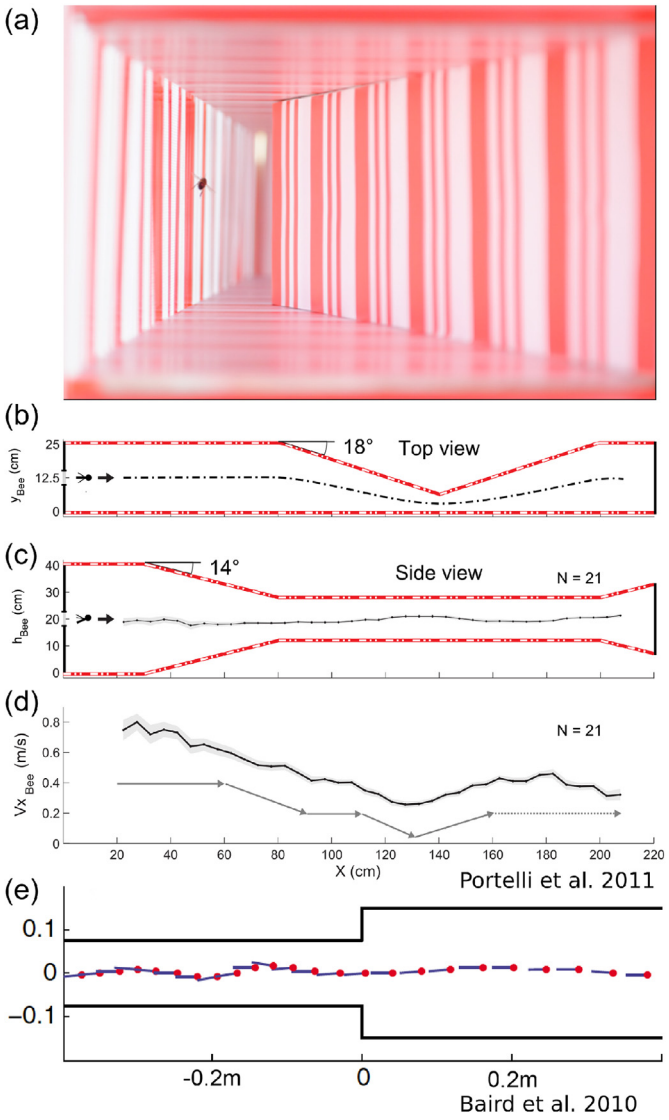


Fig. 3. (a) A honeybee flying along the doubly-tapered tunnel. The photograph was taken from the entrance of the tunnel. ©DGA/F. Vrignaux. (b) Top view of the tunnel showing the honeybee's entrance, the part tapering in the horizontal plane and the guessed trajectory of the bee in the horizontal plane with respect to the "centring response". (c) Side view of the tapered tunnel, showing the vertical constriction. The mean flight path of the honeybees is plotted as a function of the distance along the abscissa. The bees' mean trajectory can be seen to be practically vertically centered throughout the tunnel (height $h = 19 \pm 0.16$ cm). (d) Ground speed profile along the tunnel. The honeybees decreased their speed as the tunnel narrowed and increased their speed as it widened. The faded trace around the curves gives ± the standard error of the mean. The gray profile underneath the main curve shows the overall flight speed pattern as shown by the analysis. Adapted from Portelli et al. (2011). (e) The honeybees flied at low speed as the tunnel was narrow and increased their speed as it widened abruptly. Adapted from Baird et al. (2010).

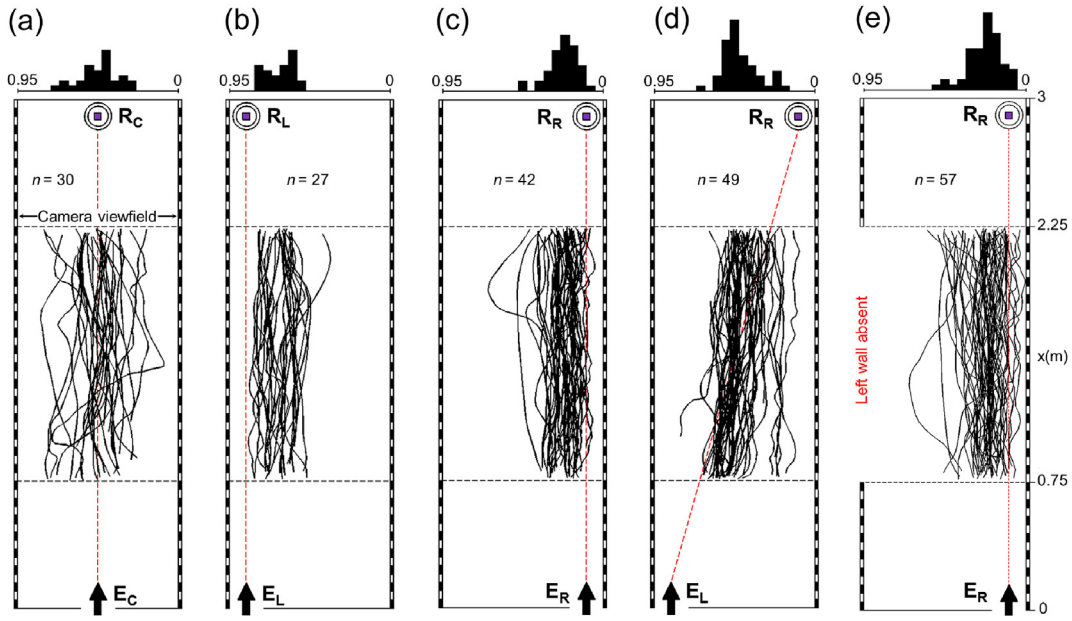


Fig. 4. Individual honeybees tested in the wide corridor (width: 0.95 m). (a) Both the bees entrance (E_C) and the feeder (F_C) were placed on the corridor midline. The mean lateral position of this set of 30 trajectories was 0.47 ± 0.11 m (±S.D.), which is very similar to the corridor midline (0.475 m) (*t* test, $p = 0.87$). (b) Entrance and feeder were both placed on the left-hand side of the corridor (E_L and F_L). The mean lateral position based on the set of 27 trajectories was 0.65 ± 0.08 m (±S.D.), which departed considerably from the midline (*t* test, $p << 0.001$). (c) Entrance and feeder were both placed on the right-hand side (E_R and F_R). The mean lateral position of the set of 42 trajectories was 0.24 ± 0.08 m (±S.D.), which again departed considerably from the midline (*t* test, $p << 0.001$). (d) Entrance and feeder were placed on opposite sides of the corridor (E_L and F_R). The mean lateral position of the set of 49 trajectories was 0.44 ± 0.11 m (±S.D.). Statistical analysis did not show a significant difference between the distributions (d) and (a) (*t* test, $p = 0.11$). (e) The bee entered the corridor and was fed on the right-hand side as in (c), but part of the left wall was removed during the trial. The histograms on top give the distribution of the mean lateral position of each trajectory. *n* is the number of trajectories recorded in each experimental condition. Adapted from Serres et al. (2007); Serres et al. (2008a).

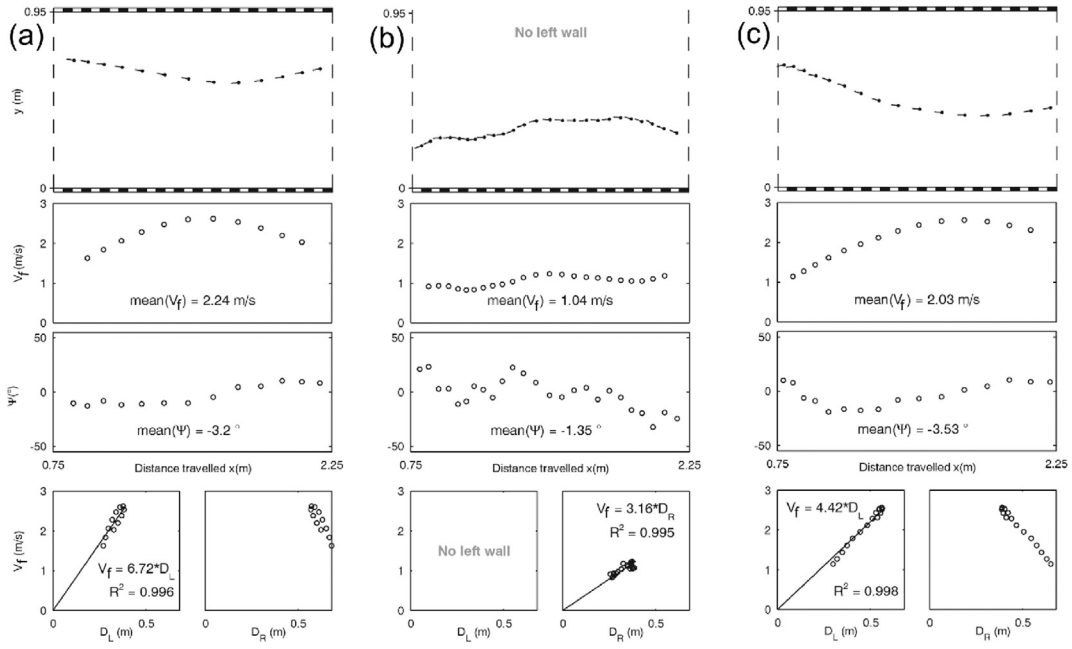


Fig. 5. Detailed analysis of three individual flight trajectories recorded in the same experiments as those shown in Fig. 4. In the top figures, the bees trajectory (*y* versus *x*) is plotted every 50 ms (dot = head; segment = body). In each case, namely (a), (b) and (c), the two middle plots give the current bee's forward speed V_f and the yaw angle ψ as a function of the distance *x* traveled in the flight tunnel. The two bottom sub-plots give the bees forward speed V_f as a function of the distance D_L from the left wall and the distance D_R from the right wall. In each case, again (a), (b), (c), the bee's forward speed V_f and the distance from one wall are proportional with a high coefficient of determination $R^2 > 0.99$. In (a) and (c), the bees forward speed V_f and its distance from the left wall D_L were found to be proportional to each other at all times. In (b), the 1.5 m long central part of the left wall was removed so that only negligible optic flow was generated on the left-hand side. The bee both entered the corridor and received its reward on the right-hand side. Its forward speed and its distance from the right wall turned out to be proportional to each other at all times, as if the bee was not in the least disturbed by the removal of the left wall. Adapted from Ruffier et al. (2007).

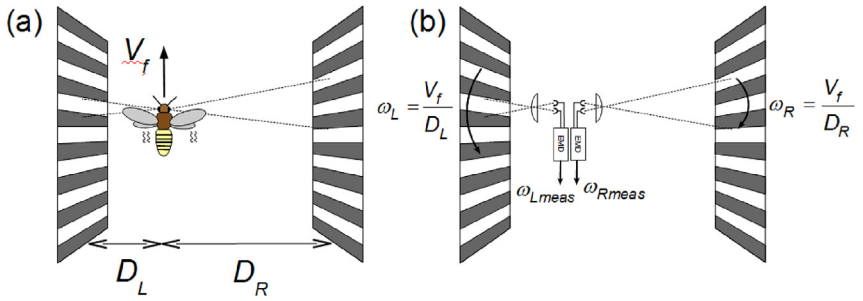


Fig. 6. (a) The right ω_R and left optic flow ω_L perceived by a bee flying in the horizontal plane along a corridor at a forward speed V_f. The bee is at a right clearance D_R and a left clearance D_L from the walls, and ω_R and ω_L are angular velocities at which two opposite points in the wall texture placed directly at a right angle seem to move. (b) By definition, ω_R and ω_L (in rad/s) are the ratios between the forward speed and the distance from the walls. A minimalistic "pair of sensitive optic flow neurons" is used inside the bee's brain: each one comprises a lens and two photoreceptors driving an Elementary Motion Detector (EMD). Each output, ω_{Rmeas} and ω_{Lmeas}, serves as feedback signals to jointly control the flight speed and lateral position.

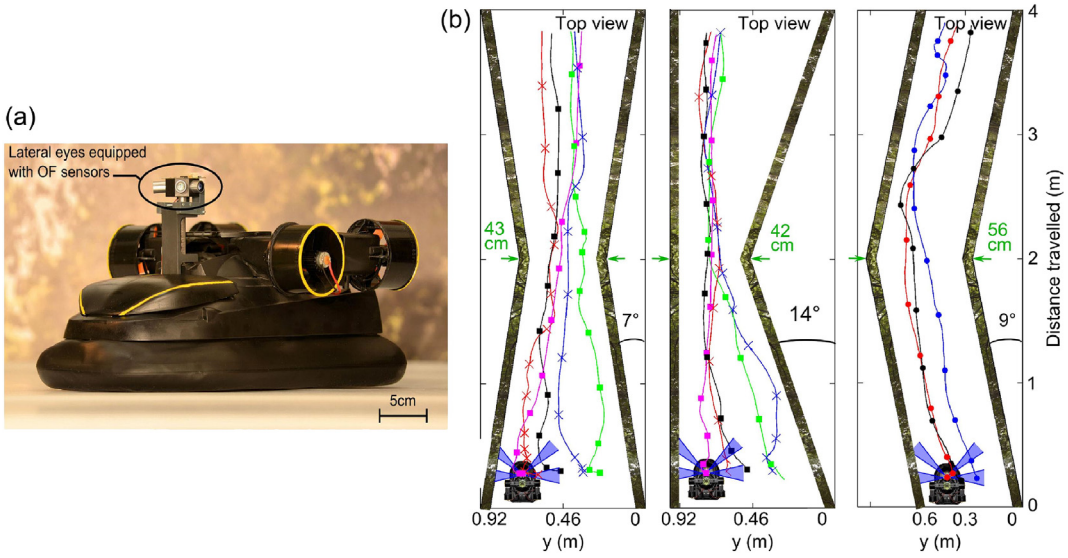


Fig. 7. (a) A fully autonomous sighted hovercraft equipped with a minimalistic (8-pixel) compound eye. (b) Automatic wall-following behaviour as a function of the initial ordinate in both tapered and bent corridors. From Roubieu et al. (2014) under CC-BY License.

doubled, the bee should fly twice as fast, or if the corridor width is halved, the bee should fly at half the speed. These kind of experiments were performed in a corridor with an abrupt change in corridor width (Baird et al., 2010; Linander et al., 2015) (Fig. 3e), and showed that bees monitored the optic flow along their lateral viewfield from 23° to 155° to control their flight speed (Baird et al., 2010) (Fig. 3e).

5.2. Optic flow balance hypothesis

25 years ago, the optic flow balance strategy was put forward to explain the bees "centring behaviour" in a narrow tunnel (Kirchner and Srinivasan, 1989; Srinivasan et al., 1991). This optic flow balance strategy was quickly applied in the field of Robotics (Coombs and Roberts, 1992) due to its Gibsonian point of view (Gibson, 1950) and thanks to its simplicity. The idea of the optic flow balance hypothesis is basically to control the heading (or the lateral position for robots that can directly act on its sway) by means of a course error as a function of an optic flow error $|\omega_L| - |\omega_R|$, where ω_L and ω_R are respectively the maximum optic flow amplitude coming from the left and the right parts of the field of view.

Fig. 4 shows trajectories of free flying honeybees in the straight corridor lined with vertical stripes. The arrows at the bottom show the bees' entrance positions (E_L, E_C, or E_R) and the circles at the top give the position of the sugar water reward (R_L, R_C, or R_R). Fig. 4a shows the bees' trajectories observed when both the entrance and the reward were centred in the corridor (E_C and R_C), the bees can be seen to have flown along the corridor midline, in agreement with honeybees "centering response" (Kirchner and Srinivasan, 1989). By contrast, bees trained to enter and collect the food near one wall flew close to this wall instead of centering along the corridor midline (Fig. 4b and c, Serres et al. (2008a)). Fig. 4d shows the trajectories taken by bees trained to collect a reward placed diagonally opposite to the entrance point (E_L and R_R), which involved crossing the corridor obliquely. A "centering response" was again observed in Fig. 4d. The results of these experiments (Fig. 4) show that bees, flying freely along a straight corridor, tend to adopt a flight path that keeps them closer to one of the walls, and do not systematically show a "centering response". In conclusion, the observed behaviour ("centering response" or "wall-following") depends on the initial position of both the entrance and the reward during the bees' training session.

Balancing optic flow in a corridor requires to measure optic flow from both sides. However, if there is only one wall, such a strategy will lead to make "the agent" to drive laterally in order to restore the visual contact with a hypothetical second wall: such a behaviour was not observed on honeybees in this particular case (see Fig. 4e). However, "wall-following behaviour" was observed to

occur in honeybees in a much wider corridor than those previously used, as well as in tunnel endowed with only one wall (Serres et al., 2008a); "centering behaviour" was observed when honeybees were trained to enter and to be rewarded along the tunnel midline (see Fig. 4a). Consequently, "centering behaviour" may occur as a particular case of "wall-following behaviour" by introducing a new optic flow-based strategy due to a Gibsonian point of view.

5.3. Unilateral optic flow regulator hypothesis

As we have seen in Fig. 4, the bees tended to follow one wall at a certain distance rather than "centering" systematically in the corridor. What strategy did the bees use to control their position laterally along the corridor? To answer this question, we analyzed a few trajectories frame by frame, selecting those where the bee made a clear-cut change of speed while crossing the 1.5 m-long observation window of the video camera. Then, the forward speed V_f as function of the distances D_L and D_R from the left and right wall was plotted to detect if there was any relationship showing that the bees relied on translational optic flow. As shown in Fig. 6a, the lateral optic flows perceived by a bee flying in the horizontal plane are the angular velocities at which the features of the environment sweep across the lateral field of view of the two eyes (Fig. 6b). The bee therefore receives a right and a left optic flow, ω_R and ω_L, respectively, which can be defined as follows:

$$\omega_R = \frac{V_f}{D_R}, \quad \omega_L = \frac{V_f}{D_L} \tag{3}$$

Fig. 5 shows three trajectories (selected among those shown in Fig. 4) in which the bee's forward speed V_f was observed to change conspicuously. In Fig. 5a, the entrance E_L was placed on the left-hand side of the corridor and the reward R_R was placed on the right-hand side. The bee's forward speed and the distance D_L from the left wall turned out to be proportional to each other throughout the 1.5 m long flight path recorded, as shown in the bottom plot (left part). By contrast, the right part of this same bottom plot (Fig. 5a) shows that the forward speed was not proportional to the distance from the right wall. In Fig. 5b, the bee entered and collected food on the right-hand side of the corridor (E_R and R_R), and the central part of the left wall was removed, so that virtually zero lateral optic flow was generated on the left-hand side. This time, it was the bee's forward speed V_f and its distance D_R from the right wall that turned out to be proportional to each other, as shown in the bottom plot. Fig. 5c gives another example showing that the forward speed V_f was proportional to the distance D_L from one wall (the left one here, as in Fig. 5a). In each case, the relationship between the bee's forward speed and the distance from either the left or right wall is almost linear, as indicated by the strong R^2-value obtained in the bottom plots of Fig. 5. According to Eq. (3), the slope of the regression line in Fig. 5 (bottom plot) is quite simply the lateral optic flow. In the three cases examined, the optic flow, as given by the slope of the regression line, was worked out at 4.42 rad/s (253°/s) in Fig. 5a, at 3.16 rad/s (181°/s) in Fig. 5b, and at 6.72 rad/s (385°/s) in Fig. 5c. Bees in Fig. 5a and b were therefore found to keep their optic flow at these values with respect to the left wall, whereas those in Fig. 5b did the same with respect to the right wall. The wall followed depended consistently on both entrance and reward positions during the bees' training session.

5.4. Dual optic flow regulator hypothesis

The first optic flow regulator was originally developed for ground avoidance when following terrain (Ruffier and Franceschini (2005); Franceschini et al. (2007), see Section 6.1). An optic flow set-point is compared to a measured optic flow to provide an error signal, this latter feeding into a regulator controlling a force orthogonal to the direction of motion. The combination of a unilateral optic flow regulator for adjusting the sway movement on either side and a bilateral optic flow regulator for adjusting the forward movement has been called a dual optic flow regulator (Serres et al., 2006, 2008b). The dual optic flow regulator concept was originally developed for aerial vehicles endowed with natural roll and pitch stabilization abilities, in which planar flight control systems can be developed conveniently (Serres et al., 2008b), in order to mimic bees' abilities in the horizontal plane (Kirchner and Srinivasan, 1989; Srinivasan et al., 1991, 1996; Serres et al., 2008a; Barron and Srinivasan, 2006; Dyhr and Higgins, 2010; Baird et al., 2010; Linander et al., 2015) (Fig. 8). The dual optic flow regulator was for the first time simulated (Serres et al., 2006, 2008b) then implemented on-board a 878-gram fully actuated hovercraft called LORA, which stands for Lateral Optic Regulator Autopilot (Roubieu et al. (2012), (2014); Fig. 7a). The dual optic flow regulator is based on:

i) a unilateral optic flow regulator that adjusts the hovercraft's lateral thrust so as to keep the higher of the two perceived lateral optic flows (left or right) equal to a sideways optic flow set-point (noted $\omega_{setSide}$). The outcome is that the distance to the nearest wall y becomes proportional to the hovercraft's forward speed V_f, as determined in (ii);
ii) a bilateral optic flow regulator adjusts the hovercraft's forward thrust so as to keep the sum of the two lateral optic flows (right and left) equal to a forward optic flow set-point (noted ω_{setFwd}).

In a steady state, with a given corridor width of D, the final operating point of the dual optic flow regulator will be:

$$V_{f\infty} = \frac{\omega_{setSide} \cdot (\omega_{setFwd} - \omega_{setSide})}{\omega_{setFwd}} \cdot D \tag{4}$$

$$y_\infty = \frac{\omega_{setFwd} - \omega_{setSide}}{\omega_{setFwd}} \cdot D \tag{5}$$

As a consequence, the robot's speed will asymptotically and automatically be scaled by the corridor width or even by the environment clutter (Fig. 7b). By increasing the forward optic flow set-point ω_{setFwd} at a given sideways optic flow set-point $\omega_{setSide}$, one can change the robot's forward speed. By reducing the sideways optic flow set-point at a given forward optic flow set-point, one can induce a graceful shift from "wall-following behaviour" to "centering behaviour". "Centering behaviour" occurs as a particular case of "wall-following behaviour", whenever $\omega_{setSide} \leq \omega_{setFwd}/2$. In addition, the dual optic flow regulator requires a third feedback loop to stabilize the robot around its vertical axis, which makes the robot experience purely translational optic flow. The robot heading is maintained constant by a heading-lock system (based on a micro-compass enhanced by a micro-gyrometer) controlling the rear thrusters differentially in closed-loop mode (Roubieu et al., 2014).

5.5. Bio-inspired visuomotor convergence hypothesis

J. Sean Humbert put forward the bio-inspired visuomotor convergence concept during his PhD (PhD thesis Humbert (2005)); obstacle avoidance and speed control (Humbert et al, 2005c; Humbert et al., 2005a); terrain-following (Humbert et al., 2005b)) explaining how to control a robot solely on the basis of optic flow. This theory is based on the spatial decompositions (Fourier's method) performed by the specific neurons in an insect's

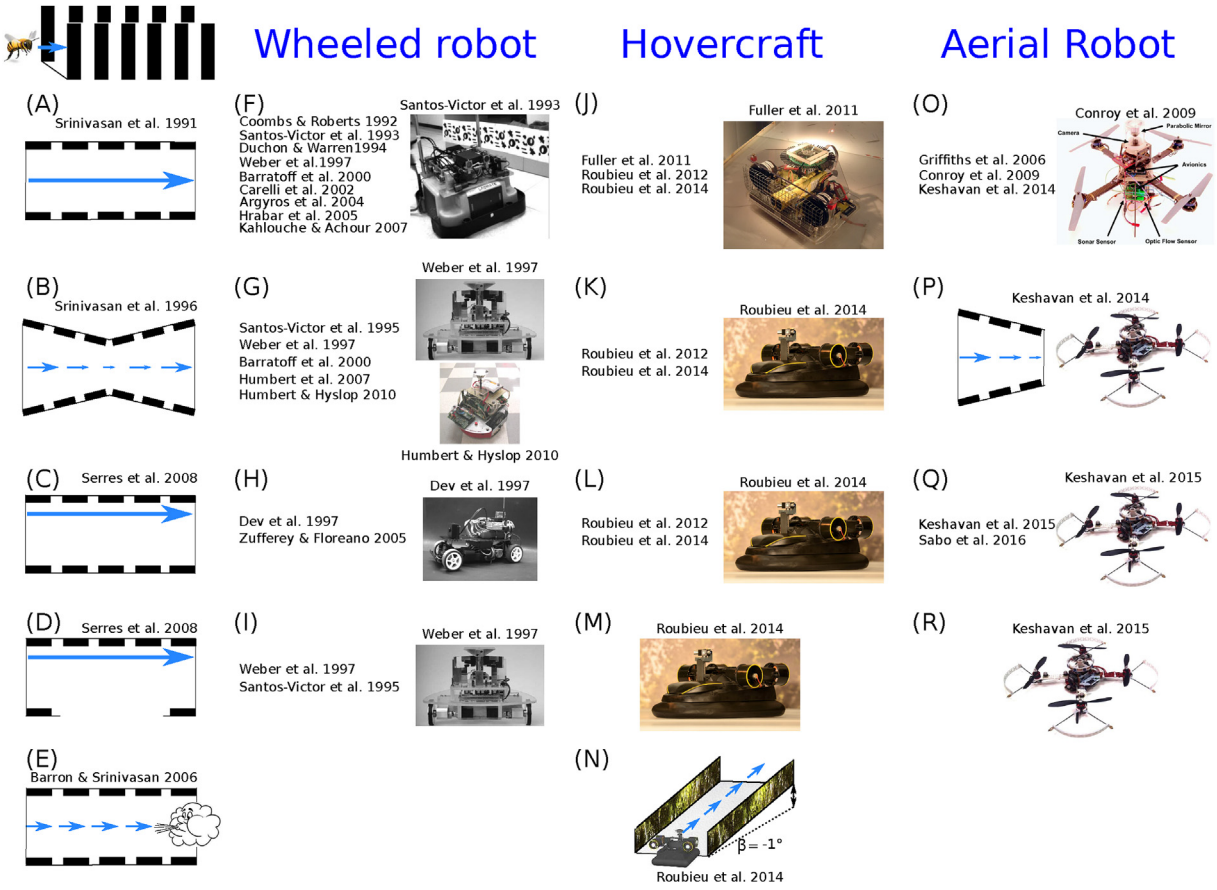


Fig. 8. Summary of the experiments on the bee's behaviours observed in the last 25 years ethological studies (A)–(E) and the various robots equipped with optic flow-based control algorithms: wheeled robots (F)–(I), robotic hovercrafts (J)–(M) and aerial robots (O)–(R). These robotic results show that optic flow-based strategies can be viewed as working hypotheses to explain how honeybees *Apis mellifera* may control both its speed and position in the horizontal plane of different tunnels. (A) Honeybees' "centring behaviour" in narrow tunnel (Srinivasan et al., 1991). (B) Honeybees' controlling speed in tapered tunnel (Srinivasan et al., 1996). (C) Honeybees' "wall-following behaviour" in wide tunnel (Serres et al., 2008a). (D) Honeybees' "wall-following behaviour" in corridor with a large opening (Serres et al., 2008a). (E) Honeybees' wind speed compensation behaviour in a wind tunnel (Barron and Srinivasan, 2006). (F) Wheeled robots exhibiting a "centring behaviour" using right and left optic flows (Coombs and Roberts, 1992; Santos-Victor et al., 1993; Duchon et al., 1994; Weber et al., 1997; Srinivasan et al., 1999; Carelli et al., 2002; Argyros et al., 2004; Hrabar et al., 2005; Kahlouche and Achour, 2007). (G) Wheeled robots exhibiting speed adjustment using bilateral optic flow (Santos-Victor et al., 1995; Weber et al., 1997; Srinivasan et al., 1999; Humbert et al., 2007; Humbert and Hyslop, 2010). (H) Wheeled robots exhibiting a "wall-following behaviour" using unilateral optic flow (Dev et al., 1997; Zufferey et al., 2005). (I) Wheeled robots exhibiting a "wall-following behaviour" using unilateral optic flow in a presence of a large opening (Weber et al., 1997; Santos-Victor et al., 1995). (J) Hovercrafts exhibiting a "centring behaviour" (Fuller et al., 2011; Roubieu et al., 2012, 2014). (K) Hovercraft exhibiting an automatic speed adjustment (Roubieu et al., 2012, 2014). (L) Hovercraft exhibiting a "wall-following behaviour" (Roubieu et al., 2012, 2014). (M) Hovercraft exhibiting a "wall-following behaviour" despite a large opening (Roubieu et al., 2014). (N) Automatic wind reaction (Roubieu et al., 2014). (O) Aerial robots exhibiting a "centring behaviour" (Griffiths et al., 2007; Conroy et al., 2009; Keshavan et al., 2014). (P) Aerial robot exhibiting automatic speed adjustment (Keshavan et al., 2014). (Q) Aerial robots exhibiting a "wall-following behaviour" (Keshavan et al., 2015; Sabo et al., 2016). (R) Aerial robots exhibiting a "wall-following behaviour" despite a large opening (Keshavan et al., 2015).

visuomotor system (see Section 3) that extract relative velocity and proximity information from patterns of optic flow.

Based on the choice of weighting function by combining the Fourier coefficients, which is an engineering analogue to the directional templates of individual Lobula Plate Tangential Cells -LPTC- neurons, various forms of relative velocity and proximity information can be obtained directly such as the lateral position and orientation (Hyslop et al., 2010) or the forward speed relative to corridor-like environments (Humbert and Hyslop, 2010). This resulting information can be applied as feedback to provide robust theoretically justified versions of the centering behaviour and automatic speed adjustment behaviour observed in flying insects. Nevertheless, it was previously demonstrated that the visual stimulation of just one fly's EMD generated a strong response of the H1-neuron, which was about 50% of its full response to thousands of EMDs (Franceschini et al., 1989). This kind of electrophysiological experiment has demonstrated that the feedback signal coming from optic flow is not as simple as a weighting function of each local optic flow measurement. This kind of nonlinearity has not yet been considered by the bio-inspired visuomotor convergence theory.

In the field of robotics, the bio-inspired visuomotor convergence was applied to a mobile robot fitted with a 1-D circular optic flow sensor providing 40 optic flow measurements (Humbert et al., 2007). The wheeled robot was able to move at up to 21 cm/s by adjusting its own speed commensurate with the local corridor width (from 2 m to 0.8 m) while following the corridor midline, even if in the presence of a 45° bend (Humbert et al., 2007). This same robot was able to negotiate a fixed-width 1.2 m corridor comprising a L-junction (Humbert and Hyslop, 2010; Hyslop et al., 2010) or in a cluttered obstacle field (Hyslop et al., 2010) at a fixed forward speed of 0.4 m/s (Humbert and Hyslop, 2010). Recently, a theoretical proof for stability of the bio-inspired visuomotor convergence theory was demonstrated on-board a quadrotor fitted with an eight-sensor optic flow ring providing 64 optic flow measurements (Keshavan et al., 2014, 2015). In addition, an analysis of the robustness and quantification of the level of uncertainty in the

environment (corridor-like environments with additional structures such as small poles, cylinders, or gaps and holes in the corridor) that the closed loop system can tolerate was provided (Keshavan et al., 2014, 2015).

Let's compare the bio-inspired visuomotor convergence theory with the optic flow balance strategy that frequently fails in corridors comprising one-sided or openings in a wall; in contrast to the switching mode strategy employed in such environments (Weber et al., 1997; Santos-Victor et al., 1995), the bio-inspired visuomotor convergence in (Keshavan et al., 2014, 2015) retains the strategy of balancing lateral optic flows and leverages the stability and performance guarantees of the closed loop to achieve stable quadrotor flight in environments that include a corridor with a large opening in a wall.

5.6. Frontal image expansion

Trajectories of flies (Land and Collett, 1974; Schilstra and van Hateren, 1999; Tammero and Dickinson, 2002; Kern et al., 2012; Censi et al., 2013) and bees (Boeddeker et al., 2010) have been found to usually consist of straight flight sequences (lasting 50–200 ms) interspersed with rapid turns termed *saccades*. Inter-saccadic sequences, in which flying insects move in the purely translation mode, enable the LPTC-neurons to assess the purely translational optic flow, which depends on several parameters including proximity information from frontal obstacles.

The optic flow balance strategy was originally suggested to explain the "centering behaviour" along a straight corridor (Srinivasan et al., 1991). However, it turned out that this strategy, when used alone, did not allow an agent to avoid frontal obstacles, i.e. following a corridor that included L-junctions or T-junctions without using the frontal viewfield (Duchon et al., 1994). The frontal image expansion can therefore be used to estimate the time-to-contact (Lee, 1976) by means of the optic flow divergence (Nelson and Aloimonos, 1988; Ancona and Poggio, 1993), and trigger a pre-specified rotation angle around the robots vertical axis. A simulated small helicopter could therefore trigger U-turns when encountering frontal obstacles (Muratet et al., 2005), or a wheeled robot could trigger a rotating angle of 90° (Duchon et al., 1994) or of 110° (Baratoff et al., 2000) in front of an obstacle, or the robot could stop and rotate on the spot until the frontal range once again became large enough (Weber et al., 1997). Other robots use a series of open-loop commands, called *body saccades*, to avoid a frontal obstacle (e.g. in Fig. 10c). The saccade duration has either been set to a constant pre-specified value (Rind et al., 2003; Zufferey et al., 2005; Zufferey and Floreano, 2006; Badia et al., 2010) (Fig. 10d), determined according to a Gaussian distribution (Reiser and Dickinson, 2003), or modulated using optic flow (Barrows et al., 2001; Green et al., 2004; Beyeler et al., 2007; Lindemann et al., 2008; Rezaei and Saghafi, 2011). Recently, an optic-flow based algorithm has been developed to compute a quantified saccade angle; this has allowed a simulated fully actuated hovercraft to negotiate tight bends by triggering body saccades, on the basis of a time-to-contact criterion and to realign its trajectory parallel to the wall along a corridor that includes sharp turns (Serres and Ruffier, 2015).

The dual optic flow regulation control scheme, which included a *saccade generator*, was also tested onboard a simulated version of the LORA Robot (Fig. 7a) in a corridor comprising a 0.8 m-wide S-shaped turn. Starting at various initial positions and orientations, our simulated hovercraft proved capable of successfully traveling along this challenging corridor (Fig. 9b). Body saccades occurred

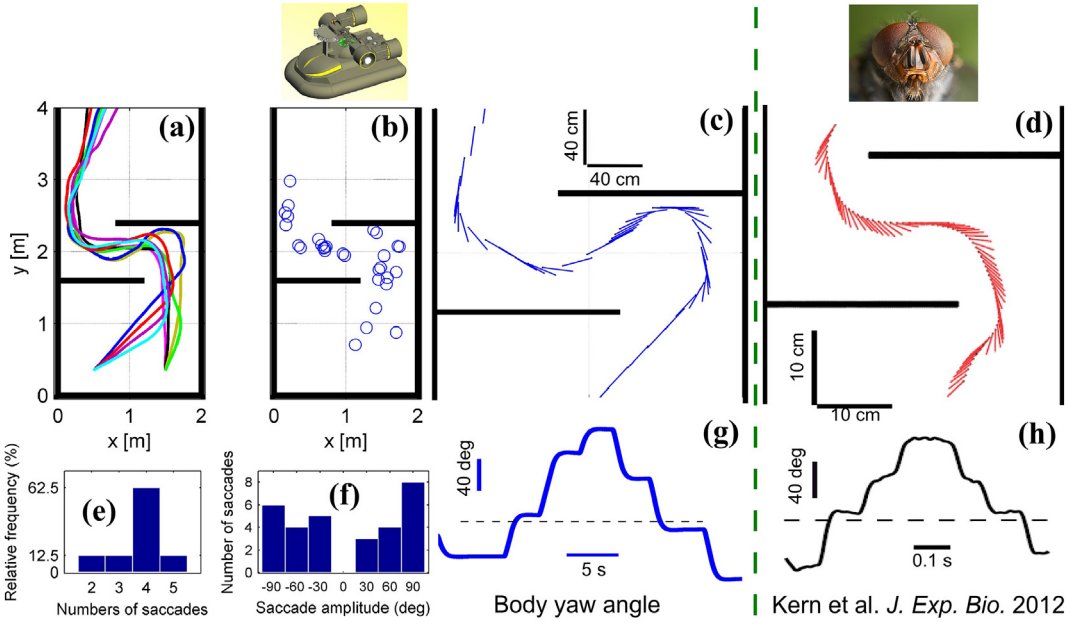


Fig. 9. Direct comparison between the behaviour of the simulated robot and that of the blowfly in an S-shaped turn. (a) 8 simulated robots trajectories in a challenging corridor comprising an S-shaped turn 0.80 m in width, starting at an initial position ($x_0 = 0.5$ m; $y_0 = 0.35$ m) with various initial orientations $\Psi_0 = (35°; 40°; 45°; 50°)$, or an initial position ($x_0 = 1.5$ m; $y_0 = 0.35$ m) and various initial orientations $\Psi_0 = (70°; 80°; 90°; 95°)$. (b) Points in the corridor at which the saccades occurred. (c) Typical trajectory of the robot among the set of 8 trajectories presented in (a). The position of the robot (black circles) and its body orientation (blue lines) are plotted every 400 ms. (d) Typical trajectory of a blowfly in an S-shaped turn, adapted from data published by (Kern et al., 2012). Position of the fly (black circles) and its long body axis (red lines) are plotted every 10 ms. Inset: head of a *Calliphoravomitoria* (Picture: J. J. Harrison, Wikimedia commons). (e) Relative frequency of saccades per trajectory while navigating the S-shaped turn ($n = 30$). (f) Body saccades were classified depending on their amplitude: −90°, between −89° and −60°, between −59° and −30°, then between 30° and 59°, between 60° and 89°, and 90°. (g) Robot's body yaw angle during the trajectory shown in (c). The horizontal dashed line gives the corridors *y*-axis ($\Psi = 90°$). (h) Fly's body yaw angle during the trajectory shown in (d). The horizontal dashed line indicates the tunnel *y*-axis ($\Psi = 90°$). Data adapted from (Kern et al., 2012). From Serres and Ruffier (2015). ©Elsevier. (For interpretation of the references to colour in this figure legend, the reader is referred to the web version of this article).

along the whole S-shaped turn (Fig. 9b), as also reported by (Kern et al., 2012) in the case of blowflies. To make some quantitative comparisons between insects and our biorobotic approach, a typical robot trajectory (Fig. 9c) was compared with a typical blowfly trajectory (Fig. 9d) in a similar corridor configuration; similar behaviour was observed in both cases, despite the huge difference in terms of the inertia. Most of the simulated trajectories involved four saccades (Fig. 9e) of various amplitudes ranging between 30° and 90° (Fig. 9f), which is on a par with the findings obtained from blowflies (Kern et al., 2012). We also compared the changes with time in the body yaw angle (in the case of the simulated robot in Fig. 9g and that of the blowfly in Fig. 9h) in an S-shaped corridor, in which 5 body yaw saccades were required to overcome the S-shaped turn. Despite the difference between the time scales in Fig. 9g and h, the body orientation profile was similar in both cases: our biorobotic approach, therefore, yielded a better understanding of this aspect of insects flight.

Centrophobism behaviour has been reported for *Drosophila*, flies avoid central zone when they are allowed to walk freely in a small square arena (Götz and Biesinger, 1985). Both visual and olfactory cues are implicated in this centrophobism behaviour (Martin, 2004) (Fig. 10a). The ability to follow the walls of a square arena on the sole basis of visual cue has been tested in simulation by using the same optic flow-based flight control system as developed in (Serres and Ruffier, 2015) (Fig. 10b). A mobile robot (Fig. 10c) equipped with a pure optic flow-based saccade generator is not able to maintain the visual contact with the walls (Fig. 10d) in comparison with the one equipped with both a dual optic flow regulator and a saccade generator (Fig. 10b). Optic flow-based strategies could be therefore able to explain how insects maintain their visual contact with the walls to follow them.

6. Short-range navigation by optic flow in the vertical plane

Ventral optic flow ω_x (expressed in rad s^{-1}) can be defined by the ratio between forward speed V_x and flight height z (Whiteside and Samuel, 1970) as follows:

$$\omega_x = \frac{V_x}{z} \tag{6}$$

The ventral optic flow can be used by aerial robots to achieve different maneuvers along the longitudinal axis: take off, terrain-following, flying nap-of-the earth, landing, decking (Fig. 12E–H). 20 years ago, a landing strategy was put forward to explain how a bee could land on flat ground (Srinivasan et al., 1996, 2000). Bees were observed to land on flat ground with a constant descent angle (Fig. 11A and B), M.V. Srinivasan and colleagues at the Australian National University therefore suggested a pair of rules for explaining the bees smooth landing on flat ground:

i) the forward speed V_f is controlled by holding the angular velocity of the image of the ground constant (i.e., holding a constant ventral optic flow $\omega_1 = \omega_2$ in Fig. 11D at 500°/s ± 268°/s (Srinivasan et al., 2000),
ii) making the instantaneous downward speed proportional to the instantaneous forward speed (Fig. 11C), i.e., holding a constant descent angle in Fig. 11A at −28°/s ± 14°/s (Srinivasan et al., 2000).

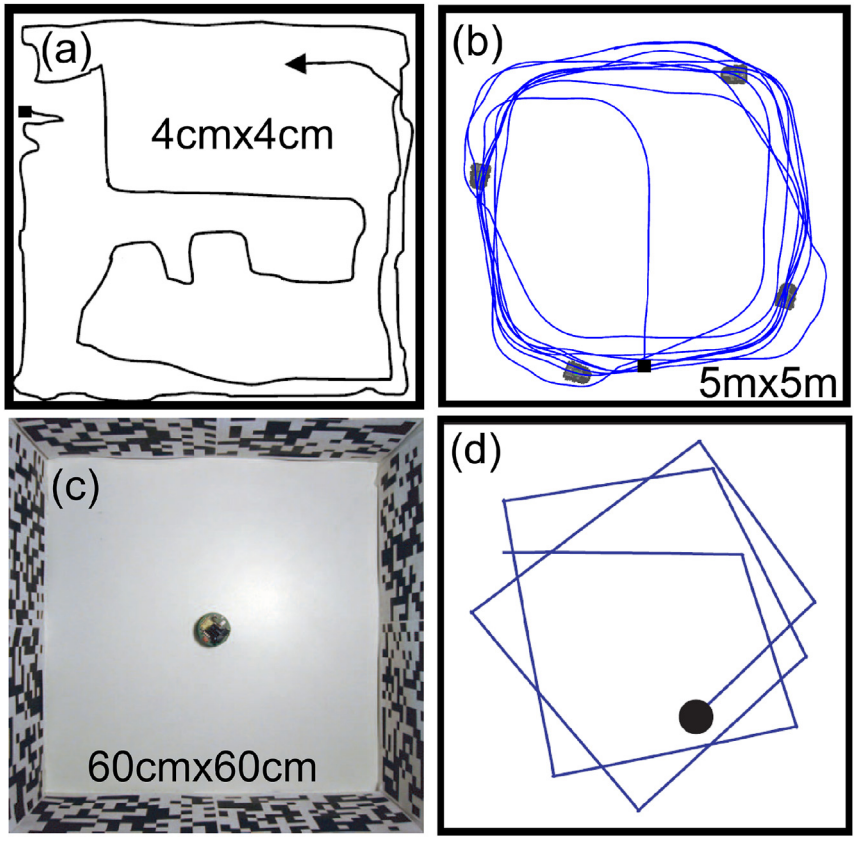


Fig. 10. (a) Centrophobism behaviour observed in *Drosophila*. Adapted from Martin (2004). ©Elsevier. (b) LORA robot inside a square arena adopting a centrophosbism behaviour by regulating the lateral optic flow combined with a *saccade generator* as described in Serres and Ruffier (2015). (c) Khepera robot in a rectangular arena (Zufferey et al., 2005), ©IEEE (d). Path of the Khepara robot in autonomous steering mode. The saccade angle is constant (90°) and it is triggered when the optic flow divergence reaches a given threshold (Zufferey et al., 2005), ©IEEE. Here, without regulating the lateral optic flow, the robot was not able to follow the walls in parallel.

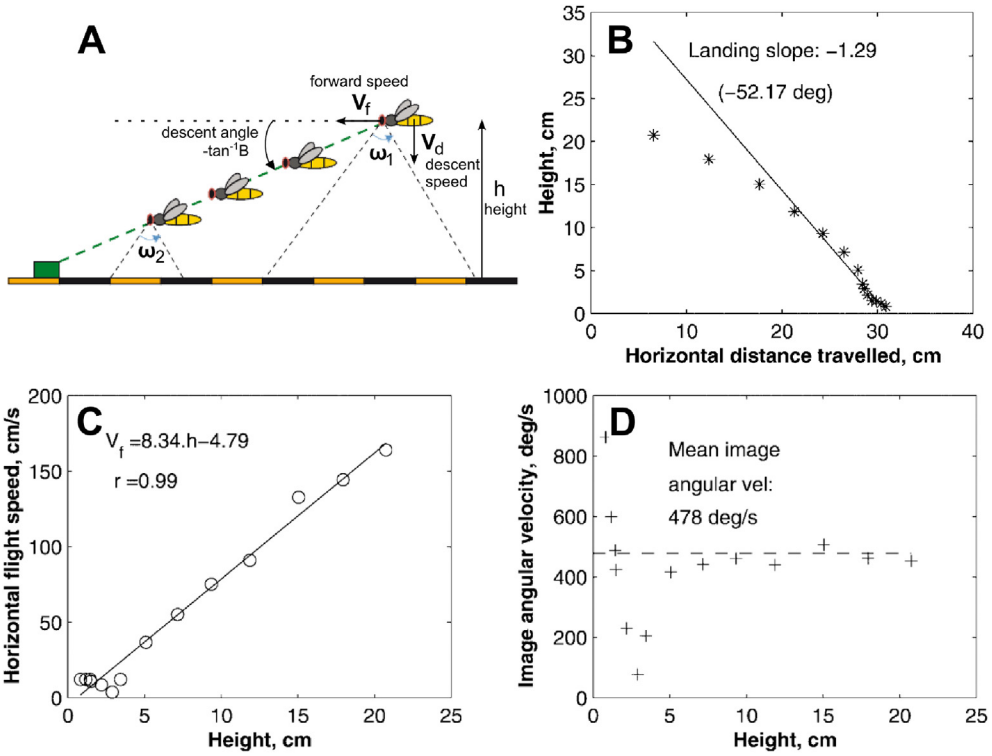


Fig. 11. (A) Parameters during a bee landing: h flight height, V_f forward speed, v_d descent speed, $\tan^{-1} B$ descent angle, ω_1 and ω_2 the optic flow for two distinct positions. Adapted from Srinivasan (2011). (B) Bee trajectory along the vertical plane with a descent angle of −52° (Srinivasan et al., 2000) ©Springer. (C) Forward speed V_f as a function of the height h showing a strong correlation between these two flight parameters (Srinivasan et al., 2000) ©Springer. (D) The ventral optic flow is maintained constant at about 478°/s during the bee's landing (Srinivasan et al., 2000) ©Springer.

This pair of rules was first implemented in a robotic gantry without including dynamic aspects (Srinivasan et al., 2000), and subsequently on-board a small fixed-wing aircraft (Chahl et al., 2004) in which the elevator angle was controlled via a proportional feedback loop by holding the ventral optic flow close to ~40°/s. During a real closed-loop flight experiment, the small fixed-wing aircraft was seen to slow down from 25 m/s to 15 m/s while losing 30 m in altitude, but experimental results were almost the same with or without the feedback loop, and the craft's altitude was observed to decrease linearly with time instead of exponentially as predicted by the pair of rules (Chahl et al., 2004). Ventral optic flow was also employed for ground avoidance on-board a Micro Air Vehicle (MAV), the mass of which was lower than 100-gram. A control algorithm based on a "bang–bang" method was used on-board a MAV to control its lift such that, if a certain threshold of ventral optic flow was exceeded, the MAV elevator angle would be moved to a preset deflection (glider in Barrows et al. (2001); fixed-wing aircraft in Green et al. (2004)).

A small Hirobo Eagle helicopter with an overall mass of 8 kg (Garratt and Chahl, 2008) used its avionics to deduce the height above ground from the ventral optic flow. The above ground height was therefore held constant by adjusting the main rotor thrust: the helicopter was able to follow the terrain at a flight height of ~1.5–2 m while flying at speeds ranging from 5 to 8 m/s (Garratt and Chahl, 2008).

6.1. Ventral optic flow regulation hypothesis

In 2003, a 100-gram tethered rotorcraft, called OCTAVE (which stands for Optic flow based ConTrol system for Aerial VEhicles, Fig. 12G), followed a smooth relief (Ruffier et al., 2003) by using the ventral optic flow regulator principle (Ruffier and Franceschini (2005), Fig. 13). A ventral optic flow regulator integrated an optic flow measurement into a feedback loop driving the robot's lift so as to compensate for any deviations in the measured optic flow from a given optic flow set-point (The OCTAVE autopilot in Fig. 13). The ventral optic flow regulator ensures that at any given moment the flight height is proportional to the groundspeed. Any increase in the groundspeed leads to an increase in height, so this can lead to an automatic takeoff then terrain-following under visual control. In the same way, any decrease in the groundspeed can lead to an automatic landing at a constant angle under visual control until touchdown at zero speed (Franceschini et al., 2007), as actually observed in honeybees in similar situations (Srinivasan et al., 1996, 2000; Srinivasan, 2011) (Fig. 12C, G). The OCTAVE robot was also able to land, along the longitudinal axis, on a moving platform (Ruffier and Franceschini, 2015), as honeybees actually do on a moving target (Zhang et al., 1990) (Fig. 12D, H).

A Vertical Take-Off and Landing (VTOL) aircraft with an overall mass of 0.85 kg (Fig. 12H, Hérissé et al. (2010)) was able to follow a steep terrain (slope 25%) at a flight height of 1.5 m while flying at 0.3 m/s by regulating the ventral optic flow at ~12°/s and estimating its own forward speed by combining both accelerometer and barometer readings (Hérissé et al., 2010).

6.2. Twin dual optic flow regulation hypothesis

With the goal of developing a full optic flow-based autopilot for 3D indoor navigation, the OCTAVE autopilot for ground avoidance (Ruffier and Franceschini, 2005) and the LORA autopilot for speed control and lateral obstacle avoidance (Serres et al., 2008b) have been combined to develop the ALIS autopilot (ALIS stands for AutopiLot using an Insect-based vision System) (Portelli et al., 2010). The ALIS autopilot consists of two visuo-motor feedback

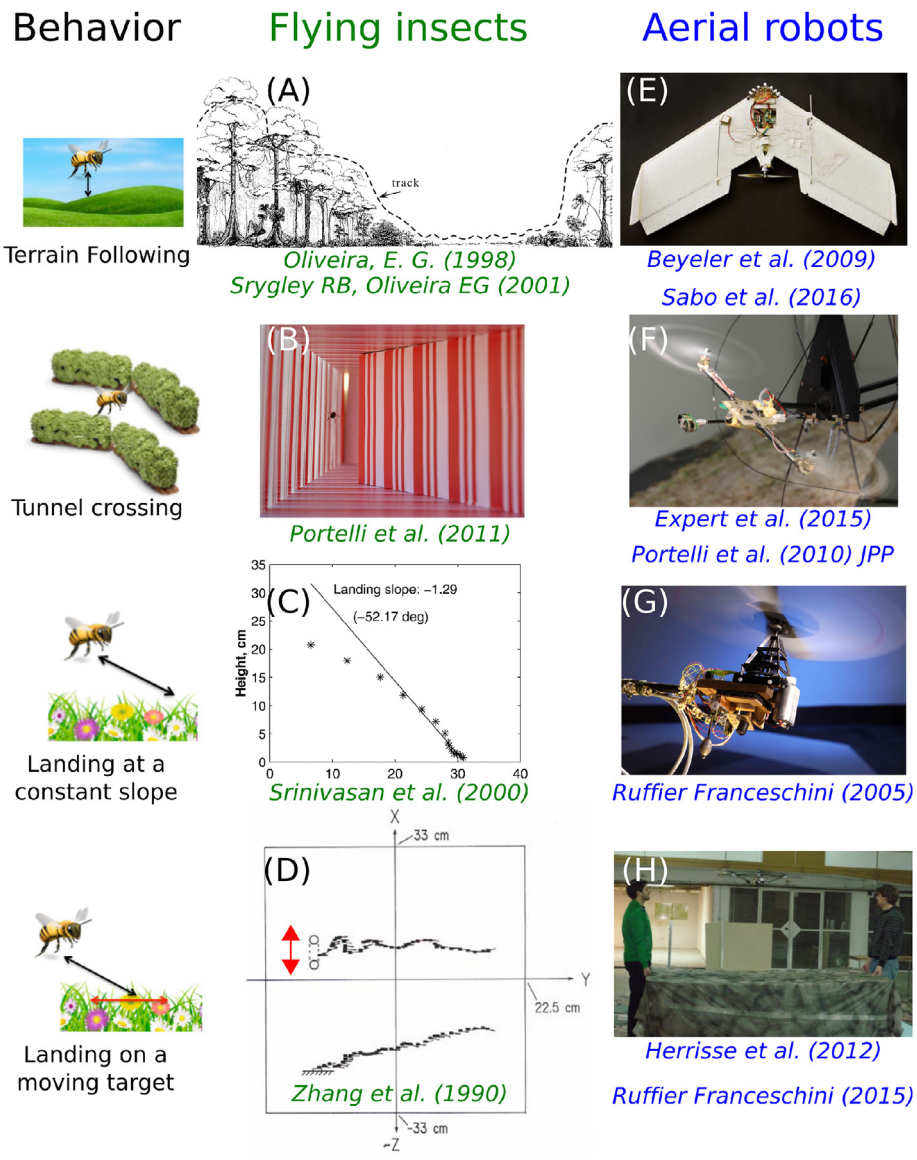


Fig. 12. Examples of the behaviour of flying insects in the vertical plane (A–D) and their robotic counterparts using optic flow (E–H). (A) Flight path of a migrating flying moth in the rainforest (de Oliveira, 1998; Srygley et al., 1999). (B) Picture of a honeybee flying in a complex double tapered corridor (Portelli et al., 2011). (C) Honeybee landing trajectory at a constant slope (Srinivasan et al., 2000). (D) Honeybee landing trajectory on a horizontally moving target (Zhang et al., 1990). (E) Free-flying aerial robot following the terrain (Beyeler et al., 2009; Sabo et al., 2016). (F) Aerial robot (Expert and Ruffier, 2015) and simulated agent (Portelli et al., 2010) following surfaces and adjusting speed in a complex tunnel. (G) Aerial robot landing at constant slope using ventral optic flow regulator (Ruffier and Franceschini, 2005). (H) Aerial robot landing on the moving platform (Herissé et al., 2012; Ruffier and Franceschini, 2015).

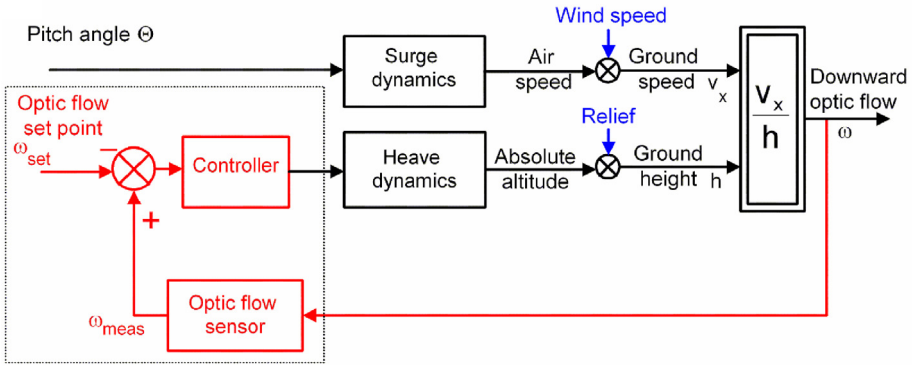


Fig. 13. OCTAVE autopilot based on a ventral optic flow regulator (OCTAVE stands for Optic flow based ConTrol system for Aerial VEhicles). The optic flow regulator controls the lift at all times so as to maintain the downward optic flow constant despite wind and relief disturbances. From Franceschini et al. (2007). ©Elsevier.

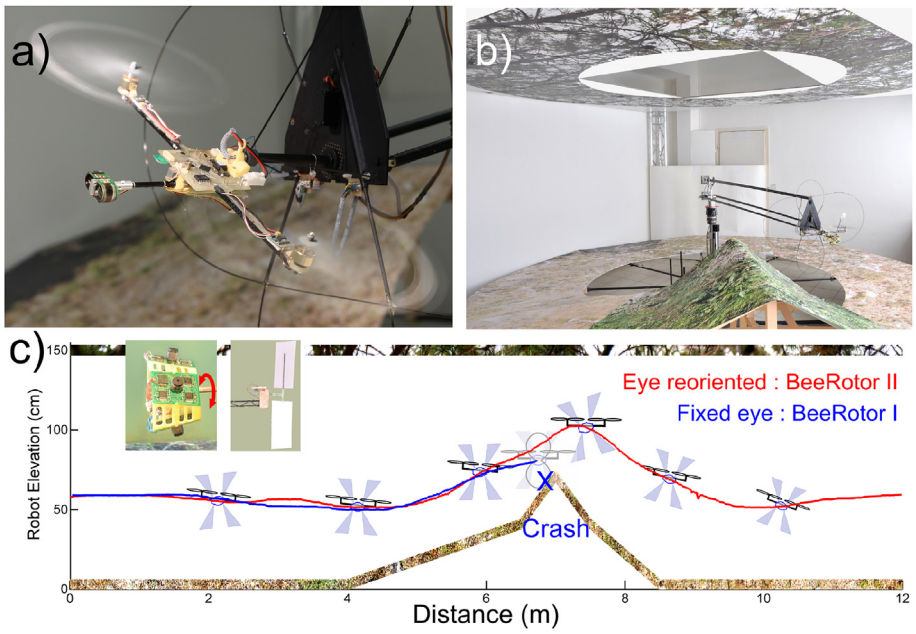


Fig. 14. (a) BeeRotor I robot equipped with the full cylindrical CurACE sensor (Floreano et al., 2013). (b) Photograph of the experimental set-up. (c) Trajectories of the robot BeeRotor II that automatically follows the ground, thanks to the ventral optic flow regulator and the fixed eye (blue) and decoupled eye (red) oriented parallel to the ground. This reorientation enables the robot, at an earlier stage, to detect the increase in the optic flow due to steep relief. Adapted from Expert and Ruffier (2015) under CC-BY license. (For interpretation of the references to colour in this figure legend, the reader is referred to the web version of this article).

loops: (i) the speed control loop (along x-axis) based on a feedback signal coming from the maximum value of the bi-lateral or bi-vertical optic flow; consequently the agent considers the minimum cross-section of the tunnel when adjusting its forward speed, and (ii) a positioning control loop (along *y*- and *z*-axis) based on a feedback signal coming from the maximum value of the lateral, ventral, or dorsal optic flow; consequently the distance from the nearest surface (lateral walls, ground, or ceiling) becomes proportional to the forward speed obtained in (i). These two loops work in parallel and are independent; each has its own optic flow set-point. Simulation results (Portelli et al., 2010) showed that an agent was able to navigate safely along a straight or tapered tunnel and to react appropriately to any untoward optic flow perturbations, such as those resulting from the occasional lack of texture on one wall or converging-diverging tunnel sections.

Recently, dual flow optic regulation in the vertical plane was tested on-board a 80-gram rotorcraft called BeeRotor (Expert and Ruffier, 2015). As a third control feedback loop, an active system of reorientation based on a quasi-panoramic eye constantly realigned its gaze parallel to the nearest surface followed: the BeeRotor robot demonstrated its abilities and achieved automatic terrain following despite steep reliefs (Fig. 14) without a need for inertial frames or scaling sensors (Expert and Ruffier, 2015).

In the framework of the Green Brain project in progress, managed by James Marshall, a dual optic flow regulator for both speed control and lateral positioning, and a ventral optic flow for altitude control were implemented on-board a small quadrotor (Sabo et al., 2016).

6.3. Ventral image expansion

The expansion of the ventral optic flow can be used for VTOL aircraft. This kind of aircraft is able to take off, hover, and land vertically. If the robot is looking straight down, the ventral image expansion can be computed by the optic flow field divergence $\nabla\overrightarrow{\omega}$ (expressed in s^{-1}), which is equal to:

$$\nabla\overrightarrow{\omega} = \omega_z = -\frac{V_z}{z} \tag{7}$$

with z the height above the ground, and V_z the ascent speed (axis pointing up). This optic flow divergence can also be expressed in terms of time-to-contact τ (expressed in s) (Lee, 1976):

$$\tau = \frac{1}{\omega_z} = -\frac{z}{V_z} \tag{8}$$

The ventral image expansion by means of optic flow divergence or time-to-contact allows a VTOL vehicle fitted with a monocular camera and an inertial measurement unit to take off, hover or land vertically without measurement of flight height or vertical speed. Methods using either an enforcement of a decreasing time-to-contact or keeping the optic flow divergence constant have been used in recent landings (Herissé et al., 2012; Izzo and Croon, 2012; Kendoul, 2014; Alkowatly et al., 2015; de Croon, 2016), as actually observed in honeybees in similar situations (Baird et al., 2013). Automatic vertical landing can be achieved using vertical optic flow (the downwards expansion of optic flow) even over a moving platform (Herissé et al., 2012; Serra et al., 2014), this kind of maneuver is called a deck-landing and could be useful for any VTOL aircraft wanting to land on the deck of a sea going vessel.

7. Optic flow is not the only visual cue used by flying insects

In this survey, we are studying on the role of motion during the generation of sensory flow and focusing on how flying insects actively shape information by behavioural strategies. Flying insects mainly use optic flow to achieve navigational tasks; however any animals in their specific ecological niches need to perceive a sensory flow to assess the environmental layout (Hofmann et al., 2013). We have limited our survey to vision in flying insects, where the optic system is, *prima facie*, restricted to fixed-focus optics lacking binocular stereopsis (Horridge, 1978). However in the early 1970s, it was found that the visual axes of the ommatidia were not

stationary (see review Viollet (2014)). It has been observed that the coordinated action of two eye muscles shifts the photoreceptor mosaic located below the facet mosaic, thus concomitantly shifting the photoreceptors' line of sight (Franceschini and Chagneux, 1997). By using a biorobotic approach, retinal microscanners were incorporated into the eye of several bio-inspired robots, which revealed major benefits in term of hyperacuity and served at the same time to test functional hypotheses about the eye muscles of flies (Viollet, 2014; Franceschini, 2014). Consequently, the previous hypothesis based on binocular stereopsis, the accuracy of which is restricted in range to a few centimeters (Horridge, 1978; Collett and Harkness, 1982; Srinivasan, 1993), have to be reconsidered from the hyperacuity phenomenon point of view for specific aerial maneuvers, such as hovering or high-speed pursuit. It has been also demonstrated that flying insects are able to follow stripes on the ground (Lehrer and Srinivasan, 1994) or stripes on the walls (Straw et al., 2010) to control their flight. Moreover, the possibility for any animal to use motion parallax as humans do to assess the three-dimensional layout of the environment was also discussed very early (Von Helmholtz, 1867; Gibson, 1958; Lee, 1974; Horridge, 1978; Collett and Harkness, 1982).

8. Conclusion

There are plenty of similar results from vertebrates and invertebrates endowed with vision, in particular those which use optic flow-based strategies (Warren, 1998; Duchon and Warren, 2002; Zeil et al., 2008). Consequently, any experiment developed for a species can be adjusted to and reused with another one to find out any similarities or discrepancies between the species. Not all common visual strategies from flying insects, animals such as birds, or even humans have yet been discovered and these should be investigated by a biorobotic approach or a transdisciplinary approach over the next decade. In addition, recent developments in insect-like robots (Fuller et al., 2014; Shyy et al., 2015) will, in the near future, allow bioroboticists to test biological hypotheses at the scale of flying insects.

Acknowledgements

The authors wish to thank David Wood (English at your Service, www.eays.eu) for revising the English of the manuscript. We thank the two anonymous reviewers for their feedback.

References

Alkowatly, M.T., Becerra, V.M., Holderbaum, W., 2015. Body-centric modelling, identification, and acceleration tracking control of a quadrotor UAV. Int. J. Model. Identif. Control 24, 29–41.
Ancona, N., Poggio, T., 1993. Optical flow from 1d correlation: application to a simple time-to-crash detector. In: 4th International Conference on Computer Vision, Proceedings of the, Berlin, Germany, pp. 209–214.
Argyros, A., Tsakiris, D., Groyer, C., 2004. Biomimetic centering behavior for mobile robots with panoramic sensors. In: Daniilides, K., Papakolopoulos, N. (Eds.), IEEE Robotics and Automation Magazine, Special Issue on "Mobile Robots with Panoramic Sensors", vol. 11, pp. 21–30.
Badia, S.B.i, Bernardet, U., Verschure, P.F., 2010. Non-linear neuronal responses as an emergent property of afferent networks: a case study of the locust lobula giant movement detector. PLoS Comput. Biol. 6, e1000701.
Baird, E., Srinivasan, M.V., Zhang, S., Cowling, A., 2005. Visual control of flight speed in honeybees. J. Exp. Biol. 208, 3895–3905.
Baird, E., Srinivasan, M.V., Zhang, S., Lamont, R., Cowling, A., 2006. Visual control of flight speed and height in the honeybee. In: From Animals to Animats 9. Springer, pp. 40–51.
Baird, E., Kornfeldt, T., Dacke, M., 2010. Minimum viewing angle for visually guided ground speed control in bumblebees. J. Exp. Biol. 213, 1625–1632.
Baird, E., Boeddeker, N., Ibbotson, M.R., Srinivasan, M.V., 2013. A universal strategy for visually guided landing. Proc. Natl. Acad. Sci. 110, 18686–18691.
Baratoff, G., Toepfer, C., Neumann, H., 2000. Combined space-variant maps for optical flow navigation. Biol. Cybern. 83 (3), 199–209.
Barron, A., Srinivasan, M.V., 2006. Visual regulation of ground speed and headwind compensation in freely flying honey bees (*Apis mellifera* l.). J. Exp. Biol. 209, 978–984.
Barrows, G., Neely, C., Miller, K., 2001. Optic flow sensors for MAV navigation. In: Fixed and Flapping Wing Aerodynamics for Micro Air Vehicle Applications, Progress in Astronautics and Aeronautics, vol. 195. AIAA, Bellingham, U.S.A., pp. 557–574
Beer, R.D., Chiel, H.J., Quinn, R.D., Ritzmann, R.E., 1998. Biorobotic approaches to the study of motor systems. Curr. Opin. Neurobiol. 8, 777–782.
Beyeler, A., Zufferey, J.-C., Floreano, D. 3d vision-based navigation for indoor microflyers. In: Robotics and Automation, 2007 IEEE International Conference on, IEEE, pp. 1336–1341.
Beyeler, A., Zufferey, J.-C., Floreano, D., 2009. Vision-based control of near-obstacle flight. Aut. Robots 27, 201–219.
Boeddeker, N., Dittmar, L., Stürzl, W., Egelhaaf, M., 2010. The fine structure of honeybee head and body yaw movements in a homing task. Proc. R. Soc. London B: Biol. Sci. 277, 1899–1906.
Borst, A., Haag, J., 2002. Neural networks in the cockpit of the fly. J. Comp. Physiol. A 188, 419–437.
Borst, A., Helmstaedter, M., 2015. Common circuit design in fly and mammalian motion vision. Nat. Neurosci. 18, 1067–1076.
Carelli,R., Soria, C., Nasisi, O., Freire, E. Stable agv corridor navigation with fused vision-based control signals. In: IECON 02 [Industrial Electronics Society, IEEE 2002 28th Annual Conference of the], vol. 3, pp. 2433–2438.
Censi, A., Straw, A.D., Sayaman, R.W., Murray, R.M., Dickinson, M.H., 2013. Discriminating external and internal causes for heading changes in freely flying drosophila. PLoS Comput. Biol. 9, e1002891.
Chahl, J., Srinivasan, M., Zhang, S., 2004. Landing strategies in honeybees and applications to uninhabited airborne vehicles. Int. J. Robot. Res. 23 (2), 101–110.
Collett, T., Harkness, L., 1982. Depth vision in animals. Anal. Vis. Behav. 111–176.
Conroy, J., Gremillion, G., Ranganathan, B., Humbert, J.S., 2009. Implementation of wide-field integration of optic flow for autonomous quadrotor navigation. Aut. Robots 27, 189–198.
Coombs, D., Roberts, K., 1992. Bee-bot: using peripheral optical flow to avoid obstacles. In: Intelligent Robots and Computer Vision XI, vol. 1825. SPIE, pp. 714–721.
de Croon, G.C., 2016. Monocular distance estimation with optical flow maneuvers and efference copies: a stability-based strategy. Bioinspir. biomim. 11, 016004.
Dev, A., Krose, B., Groen, F. Navigation of a mobile robot on the temporal development of the optic flow. In: Intelligent Robots and Systems, 1997. IROS '97., Proceedings of the 1997 IEEE/RSJ International Conference on, vol. 2, pp. 558–563.
Duchon, A.P., Warren, W.H., 2002. A visual equalization strategy for locomotor control: of honeybees, robots, and humans. Psychol. Sci. 13, 272–278.
Duchon, A. P., Warren, W. H. Robot navigation from a gibsonian viewpoint. In: Systems, Man, and Cybernetics, 1994. Humans, Information and Technology., 1994 IEEE International Conference on, volume 3, IEEE, pp. 2272–2277.
Dyhr, J.P., Higgins, C.M., 2010. The spatial frequency tuning of optic-flow-dependent behaviors in the bumblebee *Bombus impatiens*. J. Exp. Biol. 213, 1643–1650.
Egelhaaf, M., Kern, R., 2002. Vision in flying insects. Curr. Opin. Neurobiol. 12, 699–706.
Eichner, H., Joesch, M., Schnell, B., Reiff, D.F., Borst, A., 2011. Internal structure of the fly elementary motion detector. Neuron 70, 1155–1164.
Expert, F., Ruffier, F., 2015. Flying over uneven moving terrain based on optic-flow cues without any need for reference frames or accelerometers. Bioinspir. Biomim. 10, 026003.
Farrow, K., Haag, J., Borst, A., 2006. Nonlinear, binocular interactions underlying flow field selectivity of a motion-sensitive neuron. Nat. Neurosci. 9, 1312–1320.
Floreano, D., Pericet-Camara, R., Viollet, S., Ruffier, F., Brückner, A., Leitel, R., Buss, W., Menouni, M., Expert, F., Juston, R., et al., 2013. Miniature curved artificial compound eyes. Proc. Natl. Acad. Sci. 110, 9267–9272.
Floreano, D., Ijspeert, A.J., Schaal, S., 2014. Robotics and neuroscience. Curr. Biol. 24, R910–R920.
Franceschini, N., 2014. Small brains, smart machines: from fly vision to robot vision and back again. Proc. IEEE 102, 751–781.
Franceschini, N., Chagneux, R., 1997. Repetitive scanning in the fly compound eye. Göttingen Neurobiol. Rep. 2, 279.
Franceschini, N., Pichon, J.M., Blanes, C., 1992. From insect vision to robot vision. Philos. Trans. R. Soc. Lond. B Biol. Sci. 337, 283–294.
Franceschini, N., Riehle, A., Le Nestour, A., 1989. Directionally selective motion detection by insect neurons. In: Facets of Vision. Springer, pp. 360–390.
Franceschini, N., Ruffier, F., Serres, J., 2007. A bio-inspired flying robot sheds light on insect piloting abilities. Curr. Biol. 17 (4), 329–335.
Franz, M., Mallot, H., 2000. Biomimetic robot navigation. Robot. Aut. Syst. 30, 133–153.
Fuller, S. B., Murray, R. M. A hovercraft robot that uses insect-inspired visual autocorrelation for motion control in a corridor. In: Robotics and Biomimetics (ROBIO), 2011 IEEE International Conference on, IEEE, pp. 1474–1481.
Fuller, S.B., Karpelson, M., Censi, A., Ma, K.Y., Wood, R.J., 2014. Controlling free flight of a robotic fly using an onboard vision sensor inspired by insect ocelli. J. R. Soc. Interface 11, 20140281.
Gabbiani, F., Krapp, H.G., Laurent, G., 1999. Computation of object approach by a wide-field, motion-sensitive neuron. J. Neurosci. 19, 1122–1141.
Garratt, M.A., Chahl, J.S., 2008. Vision-based terrain following for an unmanned rotorcraft. J. Field Robot. 25 (4–5), 284–301.

Gibson, J., 1950. The Perception of the Visual World. Houghton Mifflin, Boston.
Gibson, J.J., 1958. Visually controlled locomotion and visual orientation in animals. Br. J. Psychol. 49, 182–194.
Götz, K.G., Biesinger, R., 1985. Centrophobism in drosophila melanogaster. J. Comp. Physiol. A 156, 329–337.
Gray, J.R., Blincow, E., Robertson, R.M., 2010. A pair of motion-sensitive neurons in the locust encode approaches of a looming object. J. Comp. Physiol. A 196, 927–938.
Green, W. E., Oh, P. Y., Barrows, G. Flying insect inspired vision for autonomous aerial robot maneuvers in near-earth environments. In: Robotics and Automation, 2004. Proceedings. ICRA'04. 2004 IEEE International Conference on, vol. 3, IEEE, pp. 2347–2352.
Griffiths, S., Saunders, J., Curtis, A., Barber, B., McLain, T., Beard, R., 2007. Obstacle and terrain avoidance for miniature aerial vehicles. In: Advances in Unmanned Aerial Vehicles. Springer, pp. 213–244.
Hartbauer, M., 2017. Simplified bionic solutions: a simple bio-inspired vehicle collision detection system. Bioinspir. Biomim. 12, 026007.
Hausen, K., 1982. Motion sensitive interneurons in the optomotor system of the fly. Biol. Cybern. 45, 143–156.
Von Helmholtz, H., 1867. Handbuch der physiologischen Optik, volume 9, Leipzig: Voss. (Translated by Southall, J.P.C. (Ed.) 1925) Helmoltz's treatise on physiological optics. Dover Publications, London. Reprinted edition 1962.
Hérissé, B., Hamel, T., Mahony, R., Russotto, F.-X., 2010. A terrain-following control approach for a VTOL unmanned aerial vehicle using average optical flow. Aut. Robots 29, 381–399.
Herissé, B., Hamel, T., Mahony, R., Russotto, F.-X., 2012. Landing a VTOL unmanned aerial vehicle on a moving platform using optical flow. IEEE Trans. Robot. 28, 77–89.
Hofmann, V., Sanguinetti-Scheck, J.I., Künzel, S., Geurten, B., Gómez-Sena, L., Engelmann, J., 2013. Sensory flow shaped by active sensing: sensorimotor strategies in electric fish. J. Exp. Biol. 216, 2487–2500.
Horchler, A.D., Reeve, R.E., Webb, B., Quinn, R.D., 2004. Robot phonotaxis in the wild: a biologically inspired approach to outdoor sound localization. Adv. Robot. 18, 801–816.
Horridge, G.A., 1978. The separation of visual axes in apposition compound eyes. Philos. Trans. R. Soc. Lond. B Biol. Sci. 285, 1–59.
Hrabar, S., Sukhatme, G. S., Corke, P., Usher, K., Roberts, J. Combined optic-flow and stereo-based navigation of urban canyons for a uav. In: 2005 IEEE/RSJ International Conference on Intelligent Robots and Systems, IEEE, pp. 3309–3316.
Humbert, J.S., 2005. Bio-inspired Visuomotor Convergence in Navigation and Flight Control Systems (Ph.D. thesis). California Institute of Technology.
Humbert, J.S., Hyslop, A.M., 2010. Bioinspired visuomotor convergence. IEEE Trans. Robot. 26, 121–130.
Humbert, J.S., Murray, R.M., Dickinson, M.H., 2005a. A control-oriented analysis of bio-inspired visuomotor convergence. In: Decision and Control, 2005 and 2005 European Control Conference. CDC-ECC'05. 44th IEEE Conference on, IEEE, pp. 245–250.
Humbert, J.S., Murray, R.M., Dickinson, M.H., 2005b. Pitch-altitude control and terrain following based on bio-inspired visuomotor convergence. In: AIAA Conference on Guidance, Navigation and Control, volume AIAA 2005-6280, San Francisco, CA.
Humbert, J.S., Murray, R.M., Dickinson, M.H., 2005c. Sensorimotor convergence in visual navigation and flight control systems. In: Proc. 16th IFAC World Congress, 38(1). Praha, Czech Republic, pp. 253–258.
Humbert, J. S., Hyslop, A., Chinnm, M. Experimental validation of wide-field integration methods for autonomous navigation. In: Intelligent Robots and Systems, 2007. IROS 2007. IEEE/RSJ International Conference on, IEEE, San Diego, CA, pp. 2144–2149.
Hyslop, A., Krapp, H.G., Humbert, J.S., 2010. Control theoretic interpretation of directional motion preferences in optic flow processing interneurons. Biol. Cybern. 103, 353–364.
Ibbotson, M., 2001. Evidence for velocity–tuned motion-sensitive descending neurons in the honeybee. Proc. R. Soc. Lond. B Biol. Sci. 268, 2195–2201.
Ijspeert, A.J., 2014. Biorobotics: using robots to emulate and investigate agile locomotion. Science 346, 196–203.
Izzo, D., Croon, G.D., 2012. Landing with time-to-contact and ventral optic flow estimates. J. Guid. Control Dyn. 35, 1362–1367.
Kahlouche, S., Achour, K., 2007. Optical flow based robot obstacle avoidance. Int. J. Adv. Robot. Syst. 4, 13–16.
Kendoul, F., 2014. Four-dimensional guidance and control of movement using time-to-contact: application to automated docking and landing of unmanned rotorcraft systems. Int. J. Robot. Res. 33, 237–267.
Kern, R., Boeddeker, N., Dittmar, L., Egelhaaf, M., 2012. Blowfly flight characteristics are shaped by environmental features and controlled by optic flow information. J. Exp. Biol. 215, 2501–2514.
Keshavan, J., Gremillion, G., Escobar-Alvarez, H., Humbert, J., 2014. A μ analysis-based, controller-synthesis framework for robust bioinspired visual navigation in less-structured environments. Bioinspir. Biomim. 9, 025011.
Keshavan, J., Gremillion, G., Alvarez-Escobar, H., Humbert, J.S., 2015. Autonomous vision-based navigation of a quadrotor in corridor-like environments. Int. J. Micro Air Veh. 7, 111–124.
Kirchner, W., Srinivasan, M., 1989. Freely moving honeybees use image motion to estimate distance. Naturwissenchaften 76, 281–282.
Koenderink, J.J., van Doorn, A.J., 1987. Facts on optic flow. Biol. Cybern. 56, 247–254.
Krapp, H.G., Hengstenberg, B., Hengstenberg, R., 1998. Dendritic structure and receptive-field organization of optic flow processing interneurons in the fly. J. Neurophysiol. 79, 1902–1917.
Krapp, H.G., Hengstenberg, R., 1996. Estimation of self-motion by optic flow processing in single visual interneurons. Nature 384, 463–466.
Lambrinos, D., Möller, R., Labhart, T., Pfeifer, R., Wehner, R., 2000. A mobile robot employing insect strategies for navigation. Robot. Aut. Syst. 30, 39–64.
Land, M.F., Collett, T., 1974. Chasing behaviour of houseflies (*Fannia canicularis*). J. Comp. Physiol. 89, 331–357.
Landgraf, T., Oertel, M., Rhiel, D., Rojas, R., 2010, October. A biomimetic honeybee robot for the analysis of the honeybee dance communication system. In: Intelligent Robots and Systems (IROS), 2010 IEEE/RSJ International Conference. IEEE, pp. 3097–3102.
Lee, D.N., 1974. Visual Information During Locomotion.
Lee, D.N., 1976. A theory of visual control of braking based on information about time-to-collision. Perception 5, 437–459.
Lehrer, M., Srinivasan, M.V., 1994. Active vision in honeybees: task-oriented suppression of an innate behaviour. Vis. Res. 34, 511–516.
Linander, N., Dacke, M., Baird, E., 2015. Bumblebees measure optic flow for position and speed control flexibly within the frontal visual field. J. Exp. Biol. 218, 1051–1059.
Lindemann, J.P., Weiss, H., Möller, R., Egelhaaf, M., 2008. Saccadic flight strategy facilitates collision avoidance: closed-loop performance of a cyberfly. Biol. Cybern. 98, 213–227.
Martin, J.-R., 2004. A portrait of locomotor behaviour in drosophila determined by a video-tracking paradigm. Behav. Process. 67, 207–219.
Muratet, L., Doncieux, S., Briere, Y., Meyer, J., 2005. A contribution to vision-based autonomous helicopter flight in urban environments. Robot. Aut. Syst. 50 (4), 195–209.
Nakayama, K., Loomis, J., 1974. Optical velocity patterns, velocity-sensitive neurons, and space perception: a hypothesis. Perception 3, 63–80.
Nelson, R., Aloimonos, J., 1988. Using flow field divergence for obstacle avoidance in visual navigation. In: Science Applications International Corp, Proceedings: Image Understanding Workshop, vol. 2.
de Oliveira, E.G., 1998. Migratory and Foraging Movements in Diurnal Neotropical Lepidoptera: Experimental Studies on Orientation and Learning (Ph.D. thesis). The University of Texas at Austin, 154pp.
Portelli, G., Serres, J., Ruffier, F., Franceschini, N., 2010. Modelling honeybee visual guidance in a 3-D environment. J. Physiol. Paris 104, 27–39.
Portelli, G., Ruffier, F., Roubieu, F.L., Franceschini, N., 2011. Honeybees' speed depends on dorsal as well as lateral, ventral and frontal optic flows. PLoS One 6, e19486.
Reiser, M.B., Dickinson, M.H., 2003. A test bed for insect-inspired robotic control. Philos. Trans. R. Soc. London A: Math. Phys. Eng. Sci. 361, 2267–2285.
Rezaei, M., Saghafi, F., 2011. Optical flow-based obstacle avoidance of a fixed-wing mav. Aircr. Eng. Aerosp. Technol. 83, 85–93.
Rind, F.C., 1984. A chemical synapse between two motion detecting neurones in the locust brain. J. Exp. Biol. 110, 143–167.
Rind, F.C., 1987. Non-directional, movement sensitive neurones of the locust optic lobe. J. Comp. Physiol. A Neuroethol. Sens. Neural Behav. Physiol. 161, 477–494.
Rind, F.C., Bramwell, D., 1996. Neural network based on the input organization of an identified neuron signaling impending collision. J. Neurophysiol. 75, 967–985.
Rind, F.C., Simmons, P.J., 1992. Orthopteran dcmd neuron: a reevaluation of responses to moving objects. i. selective responses to approaching objects. J. Neurophysiol. 68, 1654–1666.
Rind, F.C., Simmons, P.J., 1997. Signaling of object approach by the DCMD neuron of the locust. J. Neurophysiol. 77, 1029–1033.
Rind, F.C., Santer, R.D., Blanchard, J.M., Verschure, P.F., 2003. Locusts looming detectors for robot sensors. In: Sensors and Sensing in Biology and Engineering. Springer, pp. 237–250.
Rind, F.C., Santer, R.D., Wright, G.A., 2008. Arousal facilitates collision avoidance mediated by a looming sensitive visual neuron in a flying locust. J. Neurophysiol. 100, 670–680.
Roubieu, F. L., Serres, J., Franceschini, N., Ruffier, F., Viollet, S. A fully-autonomous hovercraft inspired by bees: wall following and speed control in straight and tapered corridors. In: Robotics and Biomimetics (ROBIO), 2012 IEEE International Conference on, IEEE, pp. 1311–1318.
Roubieu, F.L., Serres, J.R., Colonnier, F., Franceschini, N., Viollet, S., Ruffier, F., 2014. A biomimetic vision-based hovercraft accounts for bees complex behaviour in various corridors. Bioinspir. Biomim. 9, 036003.
Ruffier, F., Franceschini, N., 2005. Optic flow regulation: the key to aircraft automatic guidance. Robot. Aut. Syst. 50, 177–194.
Ruffier, F., Franceschini, N., 2015. Optic flow regulation in unsteady environments: a tethered mav achieves terrain following and targeted landing over a moving platform. J. Intell. Robot. Syst. 79, 275–293.
Ruffier, F., Viollet, S., Amic, S., Franceschini, N. Bio-inspired optical flow circuits for the visual guidance of micro air vehicles. In: Circuits and Systems, 2003. ISCAS'03. Proceedings of the 2003 International Symposium on, vol. 3, IEEE, pp. III–846.
Ruffier, F., Serres, J., Masson, G.P., Franceschini, N., 2007. A beein the corridor: regulating the optic flow on one side. In: Proceedings of the 7th meeting of the German neuroscience society—31st Göttingen neurobiology conference, Göttingen, Germany. Abstract T14-7B.

Sabo, C., Cope, A., Gurny, K., Vasilaki, E., Marshall, J.A., 2016. Bio-inspired visual navigation for a quadcopter using optic flow. In: AIAA Infotech@ Aerospace, p. 0404.

Santos-Victor, J., Sandini, G., Curotto, F., Garibaldi, S. Divergent stereo for robot navigation: learning from bees. In: Computer Vision and Pattern Recognition, 1993. Proceedings CVPR '93., 1993 IEEE Computer Society Conference on, pp. 434–439.

Santos-Victor, J., Sandini, G., Curotto, F., Garibaldi, S., 1995. Divergent stereo in autonomous navigation: from bees to robots. Int. J. Comput. Vis. 14, 159–177.

Schilstra, C., van Hateren, J., 1999. Blowfly flight and optic flow. i. thorax kinematics and flight dynamics. J. Exp. Biol. 202, 1481–1490.

Serra, P., Cunha, R., Hamel, T., Cabecinhas, D., Silvestre, C. Landing on a moving target using image-based visual servo control. In: Decision and Control (CDC), 2014 IEEE 53rd Annual Conference on, IEEE, pp. 2179–2184.

Serres, J., Ruffier, M.G.F., Franceschini, N., 2008a. A bee in the corridor: centering and wall-following. Naturwissenschaften 95, 1181–1187.

Serres, J.R., Ruffier, F., 2015. Biomimetic autopilot based on minimalistic motion vision for navigating along corridors comprising u-shaped and s-shaped turns. J. Bion. Eng. 12, 47–60.

Serres, J., Ruffier, F., Franceschini, N. Two optic flow regulators for speed control and obstacle avoidance. In: Biomedical Robotics and Biomechatronics, 2006. BioRob 2006. The First IEEE/RAS-EMBS International Conference on, IEEE, pp. 750–757.

Serres, J., Dray, D., Ruffier, F., Franceschini, N., 2008b. A vision-based autopilot for a miniature air vehicle: joint speed control and lateral obstacle avoidance. Aut. Robot. 25, 103–122.

Serres, J., Ruffier, F., Masson, G.P., Franceschini, N., 2007. A bee in the corridor: centring or wall-following?. In: Proceedings of the 7th meeting of the German neuroscience society—31st Göttingen neurobiology conference, Göttingen, Germany Abstract T14-8B.

Shyy, W., Kang, C.-k., Chirarattananon, P., Ravi, S., Liu, H., 2015. Aerodynamics, sensing and control of insect-scale flapping-wing flight. In: Proc. R. Soc. A, vol. 472. The Royal Society, 20150712.

Srinivasan, M.V., 1993. How Insects Infer Range from Visual Motion. Elsevier Science Ltd.

Srinivasan, M.V., 2011. Visual control of navigation in insects and its relevance for robotics. Curr. Opin. Neurobiol. 21, 535–543.

Srinivasan, M., Lehrer, M., Kirchner, W., Zhang, S., 1991. Range perception through apparent image speed in freely flying honeybees. Vis. Neurosci. 6, 519–535.

Srinivasan, M., Zhang, S., Lehrer, M., Collett, T., 1996. Honeybee navigation en route to the goal: visual flight control and odometry. J. Exp. Biol. 199, 237–244.

Srinivasan, M.V., Chahl, J.S., Weber, K., Venkatesh, S., Nagle, M.G., Zhang, S.-W., 1999. Robot navigation inspired by principles of insect vision. Robot. Aut. Syst. 26, 203–216.

Srinivasan, M.V., Zhang, S.-W., Chahl, J.S., Barth, E., Venkatesh, S., 2000. How honeybees make grazing landings on flat surfaces. Biol. Cybern. 83, 171–183.

Srygley, R., de Oliveira, E., Woiwood, I., Reynolds, D., Thomas, C., et al., September 1999. Orientation mechanisms and migration strategies within the flight boundary layer. In: Insect Movement: Mechanisms and Consequences. Proceedings of the Royal Entomological Society's 20th Symposium. CABI, London, UK, pp. 183–206.

Strausfeld, N.J., 2012. Atlas of an Insect Brain. Springer Science & Business Media.

Strausfeld, N.J., Bassemir, U., 1985. Lobula plate and ocellar interneurons converge onto a cluster of descending neurons leading to neck and leg motor neuropil in calliphora erythrocephala. Cell Tissue Res. 240, 617–640.

Straw, A.D., Lee, S., Dickinson, M.H., 2010. Visual control of altitude in flying drosophila. Curr. Biol. 20, 1550–1556.

Tammero, L.F., Dickinson, M.H., 2002. The influence of visual landscape on the free flight behavior of the fruit fly *drosophilamelanogaster*. J. Exp. Biol. 205, 327–343.

Taylor, G.K., Krapp, H.G., 2007. Sensory systems and flight stability: what do insects measure and why? Adv. Insect Physiol. 34, 231–316.

Viollet, S., 2014. Vibrating makes for better seeing: from the flys micro-eye movements to hyperacute visual sensors. Front. Bioeng. Biotechnol. 2.

Warren Jr., W.H., 1998. Visually controlled locomotion: 40 years later. Ecol. Psychol. 10, 177–219.

Webb, B., 2001. Can robots make good models of biological behaviour? Behav. Brain Sci. 24, 1033–1050.

Webb, B., 2006. Validating biorobotic models. J. Neural Eng. 3, R25.

Webb, B., Wystrach, A., 2016. Neural mechanisms of insect navigation. Curr. Opin. Insect Sci. 15, 27–39.

Weber, K., Venkatesh, S., Srinivasan, M.V., 1997. Insect inspired behaviours for the autonomous control of mobile robots. In: Srinivasan, M.V., Venkatesh, S. (Eds.), From living eyes to seeing machines. Oxford University Press, Oxford, pp. 226–248.

Whiteside, T.C., Samuel, G., 1970. Blur zone. Nature 225, 94–95.

Zeil, J., Boeddeker, N., Hemmi, J.M., 2008. Vision and the organization of behaviour. Curr. Biol. 18, R320–R323.

Zhang, S., Xiang, W., Zili, L., Srinivasan, M., 1990. Visual tracking of moving targets by freely flying honeybees. Vis. Neurosci. 4, 379–386.

Zufferey, J.-C., Floreano, D., 2006. Fly-inspired visual steering of an ultralight indoor aircraft. IEEE Trans. Robot. 22, 137–146.

Zufferey, J.-C., Floreano, D. Toward 30-gram autonomous indoor aircraft: Vision-based obstacle avoidance and altitude control. In: Proceedings of the 2005 IEEE International Conference on Robotics and Automation, IEEE, pp. 2594–2599.